



Dynamic structure-soil-structure interaction for nuclear power plants

Journal Article

Author(s):

[Kanellopoulos, Constantinos](#) ; Rangelow, Peter; Jeremic, Boris; Anastasopoulos, Ioannis; [Stojadinovic, Bozidar](#) 

Publication date:

2024-06

Permanent link:

<https://doi.org/10.3929/ethz-b-000670813>

Rights / license:

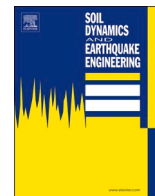
[Creative Commons Attribution 4.0 International](#)

Originally published in:

Soil Dynamics and Earthquake Engineering 181, <https://doi.org/10.1016/j.soildyn.2024.108631>

Funding acknowledgement:

813424 - INNOVATIVE GROUND INTERFACE CONCEPTS FOR STRUCTURE PROTECTION (EC)



Dynamic structure-soil-structure interaction for nuclear power plants

Constantinos Kanellopoulos^{a,*}, Peter Rangelow^b, Boris Jeremic^c, Ioannis Anastasopoulos^a,
Bozidar Stojadinovic^a

^a Department of Civil, Environmental, and Geomatic Engineering, ETH Zurich, Zurich, 8093, Switzerland

^b Section of Seismic Engineering & Dynamics, Basler & Hofmann AG Consulting Engineers, Zurich, 8032, Switzerland

^c Department of Civil and Environmental Engineering, University of California Davis, Davis, 95616, USA

ARTICLE INFO

Keywords:

Structure-soil-structure interaction (SSSI)
Nuclear power plants (NPPs)
Domain reduction method (DRM)
Nonlinear interface
Nonlinear soil
Seismic resonant metamaterials
Meta-SSI

ABSTRACT

The paper explores the linear and nonlinear dynamic interaction between the reactor and the auxiliary buildings of an idealized Nuclear Power Plant (NPP) on a realistic layered soil profile, aiming to exemplify the significance of structure–soil–structure interaction (SSSI) modelling in designing or re-evaluating critical structures, such as NPPs. Based on realistic geometrical assumptions, high-fidelity 3D finite element (FE) models of increasing sophistication are created in the Real-ESSI Simulator. Starting with elastic soil conditions and assuming tied soil–foundation interfaces, it is shown that the rocking vibration mode of the soil–reactor building system is amplified by the presence of the auxiliary building through a detrimental out-of-phase rotational interaction mechanism. Adding nonlinear interfaces, which allow for soil–foundation detachment during seismic shaking, introduces higher excitation frequencies (above 10 Hz) in the foundation of the reactor building, leading to amplification effects in the resonant vibration response of the biological shield wall inside the reactor building. A small amount of sliding at the soil–foundation interface of the auxiliary building slightly decreases its response, thus reducing its aforementioned negative effects on the reactor building. When soil nonlinearity is accounted for, the rocking vibration mode of the soil–reactor building system almost vanishes, due to the local nonlinear response of the underlying soil. This leads to a beneficial out-of-phase horizontal interaction mechanism between the two buildings that reduces the spectral accelerations at critical points inside the reactor building by up to 55 % for frequencies close to the resonant vibration frequency of the auxiliary building. This showcases the key role of SSSI modelling, and essentially implies that the neighboring buildings could offer mutual seismic protection to each other, in a similar way to the recently emerged seismic resonant metamaterials, provided that they are properly tuned during the design phase, accounting for soil and soil–foundation interface nonlinearities.

1. Introduction

Following the recent advancements in computing technology, and the development of parallel and high-performance computing (HPC) infrastructures that allow faster and more complex numerical simulations, a considerable amount of research has been devoted to the development of more realistic numerical models for soil–structure interaction (SSI) problems. Thanks to the enhanced computing power, it is yet possible to account for computationally demanding system nonlinearities, including the soil, the structure, and the various interfaces in a time-domain analysis. The importance of accounting for SSI and for such nonlinearities in earthquake engineering models is well-known and is supported by numerous studies [1–6].

The first study on SSSI was by MacCalden back in 1969 [7], who

investigated both analytically and experimentally the transmission of steady-state vibrations from one rigid circular foundation to another through the soil. Two years later, Warburton et al. [8] studied the response of two cylindrical masses on an elastic half-space, excited by a harmonic force applied to one of the masses. They showed that the interaction between the masses is maximized at frequencies associated with their resonances. In 1973, Luco & Contesse [9] were the first to introduce the term SSSI, studying the dynamic interaction between two neighboring structures, modelled as shear walls on rigid semi-circular foundations, excited by vertically propagating in-plane SH waves. Important interaction effects were observed in the case of a small shear wall structure located close to a larger one, with the response of the small structure being significantly affected by the presence of the larger structure. For more realistic 3D models, coupling between the

* Corresponding author.

E-mail address: kkanello@ethz.ch (C. Kanellopoulos).

<https://doi.org/10.1016/j.soildyn.2024.108631>

Received 3 January 2024; Received in revised form 30 March 2024; Accepted 31 March 2024

Available online 24 April 2024

0267-7261/© 2024 The Author(s). Published by Elsevier Ltd. This is an open access article under the CC BY license (<http://creativecommons.org/licenses/by/4.0/>).

horizontal, vertical, rocking, and torsional motions of the foundations should be expected. Since then, SSSI has attracted the interest of many researchers [10–18]. Gonzales [10], and Roesset et al. [11] both concluded that the interaction between structures results in coupling between different vibration modes (e.g., vertical vibrations under horizontal force) that would not appear for a single structure. They also explained that the additional inertia of one of the structures will lower the resonant frequency of the other. Betti [14] studied the dynamic interaction between embedded foundations, showing that in the lower frequency range, the translational, rocking, and torsional components of the impedance matrix exhibit clear effects of cross-interaction or coupling (up to 30 %), which decreases with increasing frequency and distance between the adjacent foundations. Padron et al. [16] studied numerically groups of structures and found that SSSI effects are important for structures of similar dynamic characteristics, resulting in either amplification or attenuation of the response. Similar conclusions have been drawn by Liang et al. [17,18], who explored 2D dynamic SSSI for twin buildings in layered half-space, for incident SH and SV waves. Recent experimental studies [19,20] provide further evidence of the significant role of SSSI in the dynamic response of adjacent structures, being either beneficial or detrimental. Thus, neglecting the interaction between two adjacent structures may not be conservative.

All of the aforementioned numerical studies assume linear soil and structure response and tied soil–foundation interfaces. There are only a few numerical studies that have attempted to account for nonlinear material behavior. Bolisetti & Whittaker [21] investigated the influence of SSSI in low- to mid-rise buildings including soil and interface nonlinearities. Although SSSI was found to be negligible in their studied cases, they concluded that future studies should further investigate the effect of nonlinear interfaces on SSSI problems. Long et al. [22] also emphasized the fact that existing numerical studies have insufficiently considered nonlinearities in their recent 2D numerical study on SSSI effects for high-rise buildings, in which they employed nonlinear models for soil, buildings, and interfaces. More recently, Kassas et al. [23] studied the effects of SSSI on the seismic response of neighboring structures on liquefiable soil, concluding that such interaction may have a major effect on the accumulation of foundation rotations and settlements.

Having reliable models, capable of realistically reproducing the seismic response of soil–structure systems under strong ground motions is of utmost importance, especially for critical infrastructure such as NPPs, where failure of nuclear safety equipment could have catastrophic consequences. As early as 1972, Lee & Wesley [24] suggested that NPPs can be designed to achieve a reduction in seismic loads by taking advantage of the interaction between neighboring structures, while improper design and layout could result in double resonance phenomena and an increase of the seismic loads. Matthees & Magiera [25] and Imamura et al. [26] also found the interaction between such massive structures to be of importance, suggesting that it cannot be disregarded. These early findings are further supported by the recent work of Roy et al. [27], who examined the impact of SSSI on the in-structure response spectra (ISRS) of a light nuclear structure adjacent to a heavy one (e.g., an emergency diesel generator building in close proximity to a reactor building). Performing linear elastic SSI analyses of the light structure using the motions adjacent to the heavier structure as input, they showed that the peak ISRS increased by a factor of 3.5, underlining the significance of SSSI. Therefore, the realistic evaluation of SSSI effects in the seismic response of new and existing NPPs is rather essential, requiring advanced numerical simulations that account for nonlinearities in the entire dynamic system. Although such nonlinear SSI effects on NPP equipment have been studied for a single nuclear reactor building in the past few years [28–31], to the best of our knowledge, the nonlinear SSSI effects on the seismic response of NPP equipment have not been systematically addressed.

The studies discussed above have clearly demonstrated the importance of considering nonlinear SSSI effects for adjacent structures in

NPPs. Aiming to contribute towards bridging the existing knowledge gap, a high-fidelity 3D finite element (FE) model of an idealized NPP is developed, consisting of the main reactor building and an auxiliary building that surrounds it. The objective of this paper is to describe the nonlinear time–domain SSSI analysis method, its key components (e.g., interface and soil material nonlinearities) and the necessary assumptions, and to demonstrate the SSSI effect through the analysis of the results. It should be noted that the results presented at this stage do not aim to address the aleatory uncertainties that are crucial in design practice or to provide definitive quantitative measures for design. Instead, they serve as a proof-of-concept for a nonlinear time–domain SSSI model and its advantages for modelling and analysis of the complex seismic responses of adjacent NPP buildings and their interactions. The results are presented in two stages: first, the response of the idealized NPP reactor building with or without the presence of the auxiliary building is explored, progressively increasing the level of FE analysis sophistication. A linear elastic analysis is initially conducted, followed by the introduction of nonlinear soil–foundation interfaces, and finally of nonlinear soil response. In this way, it is possible to explore the role of each nonlinearity and to quantify its impact on SSSI and building responses. Second, the effect of the auxiliary building on the seismic response of the reactor building and its equipment is explored for all levels of FE analysis sophistication, with emphasis on critical internal components, such as the reactor vessel.

2. Methodology

To investigate the dynamic interaction between the NPP reactor building and the auxiliary building, a detailed 3D FE model is implemented in the Real-ESSI Simulator [32]. Real-ESSI provides state-of-the-art tools for computational modelling in earthquake engineering, enabling the development of realistic models of earthquakes, soils, structures, and their interactions (ESSI). Such tools include the domain reduction method (DRM), which allows simulation of all types of seismic waves (as explained in more detail later); a variety of advanced constitutive models to simulate the nonlinear response of soils, structures, and their interaction; analytical probabilistic modelling tools; analytical calculation of all energy variables to monitor how the energy is distributed in the model; and parallel computing capabilities.

Fig. 1 shows an overview and a cross-sectional view of the 3D FE NPP–soil model, portraying the idealized NPP reactor building positioned at the center, surrounded by the auxiliary building. The two buildings are on separate foundations and are not in direct contact with each other, having a clearance of 1 m. In reality, the clearance between such structures is significantly smaller (typically 0.1–0.2 m). However, in order to ensure a computationally stable simulation with a reasonable element size, a 1 m clearance is assumed. The FE mesh is generated using the open-source mesh generator Gmsh [33]. All simulations were performed on the Euler parallel computing cluster, operated by the ETH Zurich High-Performance Computing group. The results are visualized with ParaView [34]. A detailed description and verification of individual model components is offered below.

2.1. Domain reduction method (DRM)

The domain reduction method is a simple, yet powerful numerical technique that allows realistic simulation of all seismic (body and surface) waves in a reduced domain, comprising only the structure(s) and soil layers of interest. Originally developed by Bielak et al. [35,36], it aims at bridging the gap between seismologists and earthquake/civil engineers. Seismologists develop regional simulation models of earthquakes, focusing on modelling the fault rupture and the subsequent wave propagation through the earth's crust to a site of interest, without considering the structure(s). In contrast, earthquake engineers study a much smaller domain, containing only the structure(s) and the local soil of interest, (over)simplifying the input seismic waves to 1-, 2- or

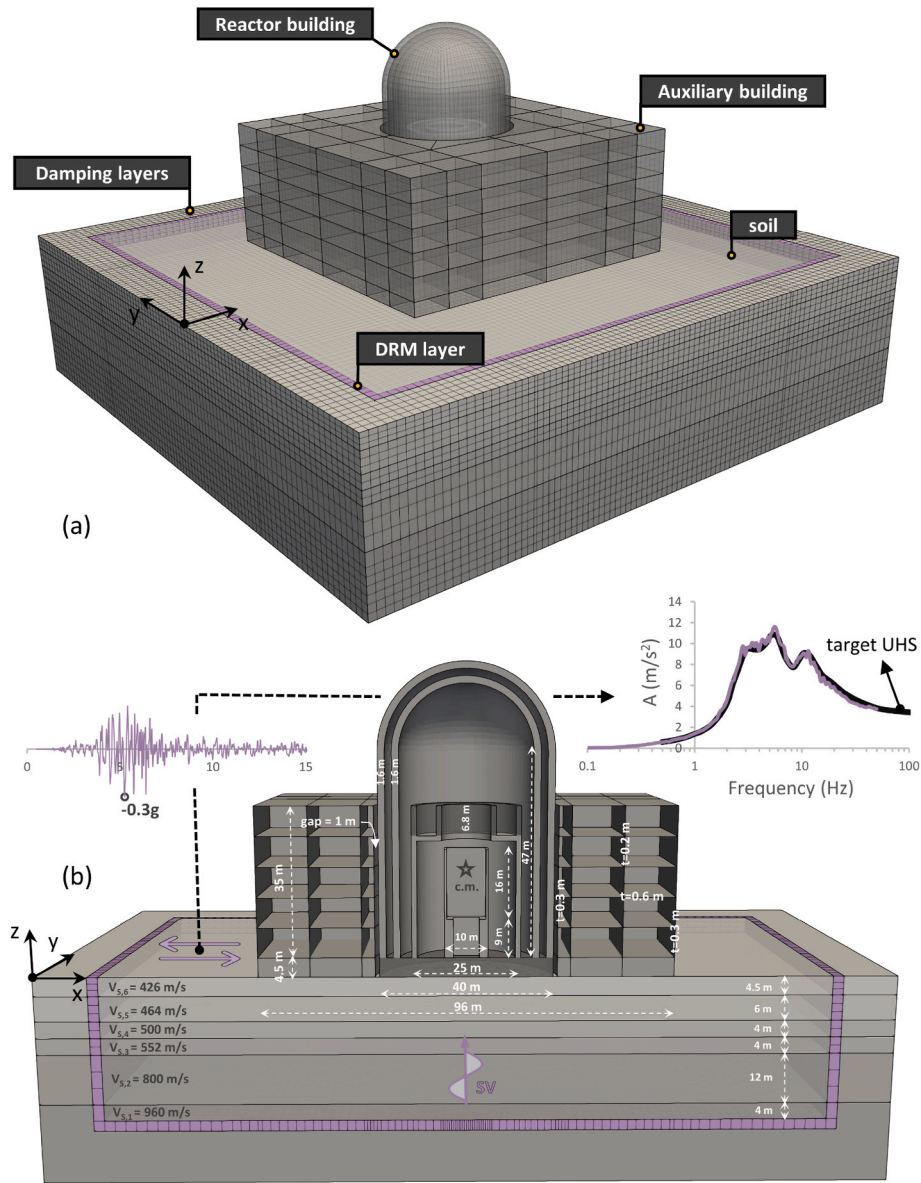


Fig. 1. (a) Overview of the 3D DRM FE model of the idealized NPP and the reduced soil domain; and (b) cross-section of the model, showing key geometric and material properties. An artificial accelerogram is reproduced at the ground surface using the DRM forces applied at the reduced domain boundary (DRM layer).

3-component motions, by shaking horizontally and vertically the base of their models. Such engineering approach may produce the desired acceleration time histories at the ground surface, but it assumes that all ground surface points move identically, which may not be realistic depending on the problem being studied. With the DRM, it is possible to input arbitrary 3D seismic waves generated by the regional simulation model into the reduced domain model of interest, which can also be nonlinear, by applying equivalent effective seismic forces on the reduced domain (Fig. 1), calculated according to the DRM theory. To attenuate the radiated waves resulting from the vibration of the structures in the reduced domain model, a few layers of elastic damping elements with progressively increasing damping properties are required to surround the reduced domain model and the DRM elements. If no structures are modelled (free-field), no waves are expected to leave the reduced domain model, resulting in zero displacements of the damping elements.

Since regional earthquake model data is limited due to its high computational cost and required knowledge of regional seismotectonics and geology, this study utilizes DRM to generate a one-component wave

field of vertically propagating horizontal shear waves (SV), which is a typical simplification in the nuclear industry [37]. For this purpose, Real-ESSI assumes that the regional earthquake model of the first DRM step is an one-component wave propagation model in a layered half-space, which can be solved analytically to calculate the effective DRM forces. These forces are then applied during the second DRM step (main time history analysis) on the DRM nodes (Fig. 1) to input the one-component SV waves in the soil domain (i.e., *in-plane* motion – soil particles motion parallel to x direction). To damp out any radiation waves produced by the oscillation of the buildings, five rows of damping elements with increasing Rayleigh damping from 0 % to 100 % are modelled around the reduced domain.

In this study, an artificial ground motion compatible with the “ENSI-2015” [38] mean uniform hazard spectrum for an NPP site in Switzerland with an annual exceedance frequency of 10^{-4} is defined at the ground surface. Using the DRM approach, the seismic actions are transferred to the DRM nodes as equivalent effective forces. This single-component (horizontal) motion is considered sufficient in this study. In the case of an actual design or re-evaluation project of a new or

an existing NPP, respectively, engineering practice would dictate the use of multiple sets of 3D acceleration time histories as SSSI is a three-dimensional phenomenon.

2.2. NPP reactor building

The 71.5 m tall idealized NPP reactor building is located at the center of the model, with its containment structure comprising two reinforced concrete (RC) shells; an outer shell and a pre-stressed inner shell. Each shell is 1.6 m thick, with radii of 20 m and 16.8 m for the outer and inner shells, respectively. A 35 m high cylindrical RC wall (CW) with a 12.5 m radius is inside the reactor building and supports a water pool (WP). In addition, in the center of the reactor building there is a 16 m high biological shield wall (BSW), within which the reactor vessel (RV, here not explicitly modelled) sits on a 9 m high reactor vessel pedestal (RVP). Both structures are simplistically assumed to be square reinforced concrete prisms; BSW is 0.5 m and RVP is 2 m thick, respectively. These two critical reactor building components are associated with the dynamic behavior of the reactor vessel, and are thus simply referred to as the reactor vessel (RV). The reactor building is supported by a circular 4.5 m thick RC foundation. This foundation is not connected to the foundation of the auxiliary building. A configuration such as this one is found in many NPPs worldwide, as a common foundation mat—although desirable—has not been the selected solution for various reasons.

The reactor building is modelled using linear elastic 8-node brick elements with typical RC material properties: Young’s modulus $E_{RC} = 35$ GPa; Poisson’s ratio $\nu_{RC} = 0.17$; and unit weight $\rho_{RC} = 2.55$ Mg/m³. To roughly account for the additional mass of the heavy permanent equipment on the foundation level and of the water inside the water pool, the unit weight of the foundation and the water pool is increased to 5 Mg/m³, as indicated by the darker grey color in Fig. 1b. As a result, the center of mass of the reactor building is at 25 m above the ground surface, while its total weight is approximately 100,000 Mg. A typical 7 % viscous Rayleigh damping (mass proportional coefficient $\alpha_0 = 2.2$ s⁻¹, stiffness proportional coefficient $\alpha_1 = 0.00124$ s) is assigned to the outer containment wall, and 4 % ($\alpha_0 = 1.26$ s⁻¹, $\alpha_1 = 0.000707$ s) to the inner wall, which is assumed to be prestressed—hence the lower damping value [37].

As a first step in understanding the dynamic behavior of the NPP reactor building, an eigenvalue analysis of the fixed-base reactor building is performed. Fig. 2 displays the fundamental translational vibration modes of various components of the reactor building along with their corresponding eigenfrequencies. The eigenfrequencies of the first translational vibration modes of the containment walls, the CW, and the RV, which are of significant interest in this study, are approximately 4, 5, and 12 Hz, respectively. The second translational vibration modes of the containment walls and the RV are also presented for reference. To

assess the adequacy of the current FE mesh discretization, which employs linear 8-node brick elements, the same reactor building model was discretized with more accurate—but computationally more expensive—quadratic linear elastic 27-node brick elements. The deviation from the translational vibration modes of interest displayed in Fig. 2 was found to be less than 5 %, indicating that the linear 8-node brick elements provide sufficient accuracy.

2.3. Auxiliary building

Typically located adjacent to the reactor building, auxiliary buildings are essential structures for the safe and efficient operation of NPPs, as they house important equipment, such as the radioactive waste systems, the chemical and volume control systems, and the emergency cooling water systems. In this particular study, an idealized 4-storey, 39.5 m tall and 96 m wide square RC auxiliary building surrounds the reactor containment structure (Fig. 1). It is founded on a 4.5 m thick separate RC foundation. The circular opening in the center has a 21 m radius to fit the reactor building. The internal walls, slabs, and external RC walls are 0.2 m, 0.6 m, and 0.3 m thick, respectively.

Except for its foundation, the auxiliary building structure is modelled using linear elastic 4-node shell elements with 6 degrees-of-freedom (dofs) per node. The foundation consists of linear elastic 8-node brick elements with 3 dofs per node. To ensure that the walls are fixed at the top of the foundation, a master-slave kinematic constraint is applied on the translational dofs of the common nodes between the foundation and the embedded walls. All elements of the auxiliary building are assigned the same RC material properties as the reactor building (except for the embedded portions of the walls, which have an almost zero unit weight). The auxiliary building has a total weight of about 180,000 Mg and is assigned a Rayleigh damping of 7 % ($\alpha_0 = 2.2$ s⁻¹, $\alpha_1 = 0.00124$ s).

Fig. 3 presents the first three vibration modes of the fixed-base auxiliary building. The focus of this study is on the first translational mode, which has an eigenfrequency of about 6 Hz. The second torsional vibration mode and the third one, which involves slab vibration, are less relevant as the interaction between the two buildings is mainly through their translational and rocking vibration modes, as demonstrated later on.

It should be noted that both the reactor and the auxiliary building models were assumed to respond within the elastic range for the considered seismic hazard levels, in accordance with the standards for safety-related NPP structures [37,39]. The mechanical characteristics of the finite elements and their damping ratio values were selected accordingly.

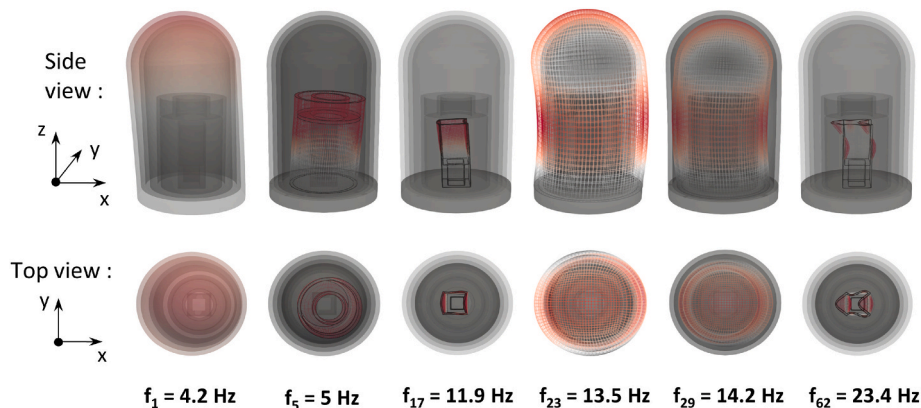


Fig. 2. Side views (top) and top views (bottom) of the fundamental translational eigenmodes of the fixed-base case of the reactor building, and the corresponding eigenfrequencies.

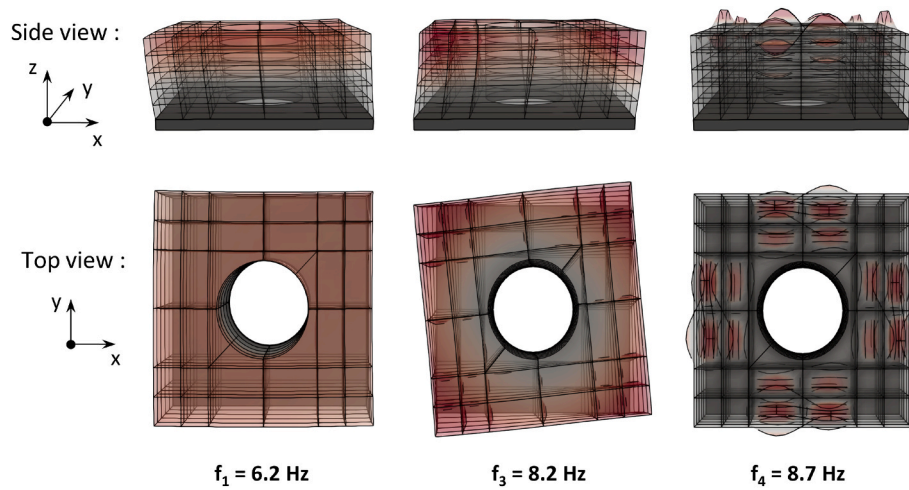


Fig. 3. Side views (top) and top views (bottom) of the first three eigenmodes of the fixed-base case of the auxiliary building, and the corresponding eigenfrequencies.

2.4. Soil

The reactor and the auxiliary building structures are founded on the ground surface of a realistic soil profile, representative of a central-European NPP site [40]. As the embedment of these two structures was assumed to be shallow, its effect was neglected [37] due to the low confining pressure and the consecutive soil–basement wall separation after a few earthquake cycles.

2.4.1. Linear elastic soil

The soil profile consists of six layers of increasing shear wave velocity with depth. The shear wave velocity V_s , the unit weight ρ , the Poisson's ratio ν , and the thickness h of each soil layer are summarized in Table 1. Linear elastic 8-node brick elements are employed to model the soil, with at least 10 elements per wavelength [41], assuming that the maximum frequency of interest is 20 Hz. A Rayleigh damping of 2% ($\alpha_0 = 0.628 \text{ s}^{-1}$, $\alpha_1 = 0.000354 \text{ s}$) is assumed, which is typical for linear elastic soil conditions [42].

Therefore, the selected mesh discretization is theoretically able to simulate the propagation of vertical shear waves of up to 20 Hz. To verify this claim, a simplified analysis of a soil column with the same soil layers and mesh discretization as the main model is conducted. Indeed, employing the DRM, the targeted acceleration time history and pseudo-acceleration spectrum (SA) (denoted as input in Fig. 4) can be successfully reproduced at the ground surface (denoted as output in Fig. 4) even for up to 30 Hz.

2.4.2. Nonlinear soil

Linear elastic or equivalent-linear approaches are considered a good starting point for understanding complex dynamic SSSI problems. Such methods have been widely used in both research and practice over the past decades, mainly due to their ease of use and their reduced computational cost. However, soil behavior is known to be inherently nonlinear [43] (even at small strains) making the equivalent-linear approach unsuitable for modelling the soil response to strong ground

motions. Furthermore, as will be shown later on, ignoring the nonlinear response does not always lead to conservative results. Therefore, it is imperative to investigate the dynamic response of NPP structures using a nonlinear soil model [44].

In this context, an elastoplastic constitutive model is employed, incorporating a von Mises failure criterion, the Armstrong–Frederick nonlinear kinematic hardening [45], and an associated flow rule. Such model is relatively simple but robust and effective in simulating pressure-independent materials. Similar constitutive models have been broadly adopted in research in recent years [46,47]. Table 2 summarizes the parameters of the constitutive model for all soil layers, where ρ , E , and ν are following Table 1; R is the radius of the deviatoric section of the von Mises yield surface that controls the size of the elastic region; and h_u and c_r are two parameters that control the post-yield hardening behavior, with their ratio h_u/c_r being calibrated to achieve the target undrained shear strength S_u , which is not a parameter of the model. The target S_u for each soil layer is defined assuming that the ratio of shear modulus to undrained shear strength G_0/S_u is equal to 800—a typical value [48]—except for the surface soil layer, which is usually improved, and hence a lower value of $G_0/S_u = 500$ is chosen. In addition to the hysteretic damping stemming from nonlinear soil response (plastic energy dissipation), a viscous Rayleigh damping of 2% ($\alpha_0 = 0.628 \text{ s}^{-1}$, $\alpha_1 = 0.000354 \text{ s}$) is assumed to crudely account for the viscous energy dissipation caused by the soil–pore fluid interaction.

To validate the employed constitutive model at the element level, a single element of each soil layer is subjected to cyclic shear loading of increasing amplitude. For each layer, the computed normalized secant shear modulus – shear strain ($G/G_0 - \gamma$) curve is compared with experimental data from the specific site [40]. Such a comparison is illustrated in Fig. 5, which compares the numerical and experimental $G/G_0 - \gamma$ curves for the 2nd soil layer. Despite its fluctuations, the numerical curve remains within the upper and lower bounds of the experimental curve for the specific site, for the entire strain range. Almost identical plots were obtained for all other soil layers, validating the selected parameters of the constitutive model. Finally, to estimate the expected level of inelasticity in each soil layer due to the propagating shear waves, a nonlinear soil column is modelled and subjected to the previously discussed artificial acceleration time history. The resulting vertically propagating shear waves (SV) entering the model reproduce the target acceleration time history at the top of the soil. Fig. 6 depicts the shear stress – shear strain ($\tau - \gamma$) response hysteresis loops for each soil layer. The maximum shear strain observed is slightly less than 3×10^{-4} , which can be considered a fairly inelastic behavior, corresponding to G/G_0 of about 0.6. However, it should be noted that locally, under the edges of the reactor and auxiliary building RC foundations, a higher

Table 1

Elastic material properties of the layered soil profile.

Soil Layers	V_s (m/s ²)	ρ (Mg/m ³)	ν (–)	h (m)
6	426	2	0.4	4.5
5	464	2	0.4	6
4	500	2	0.4	4
3	552	2.2	0.4	4
2	800	2.2	0.4	12
1	960	2.65	0.4	4

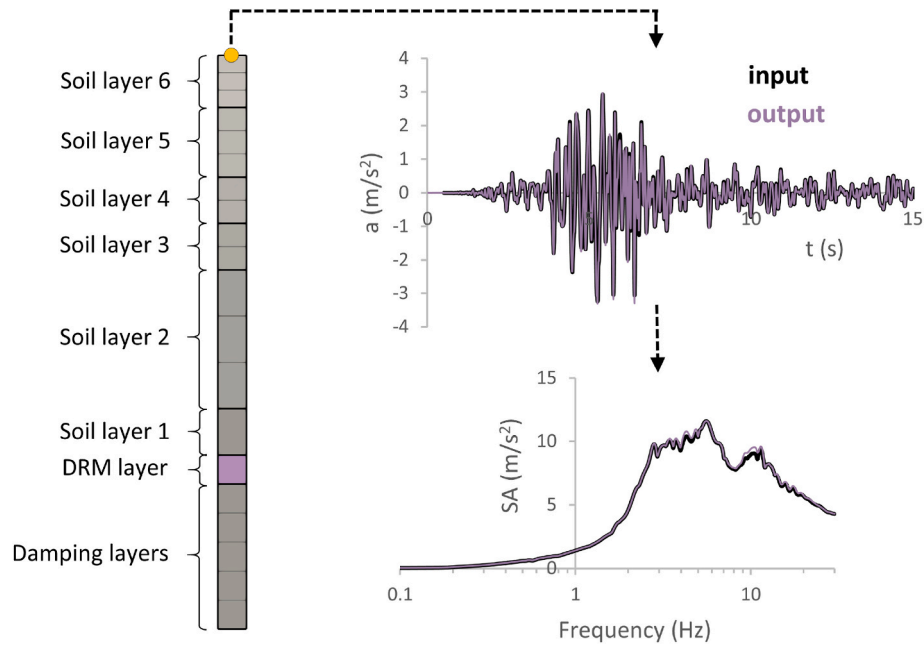


Fig. 4. Verification of vertical wave propagation (one-component SV waves) in a linear elastic soil column using the DRM. Comparison of the requested (input) to the resulting (output) acceleration time histories at the ground surface (top) with their corresponding spectral acceleration plots (bottom).

Table 2

Input parameters of the Von Mises elastoplastic model with Armstrong-Frederick nonlinear kinematic hardening for each soil layer, along with the corresponding undrained shear strength S_u and the thickness h for each layer.

Soil Layers	E (MPa)	ρ (Mg/m ³)	ν (-)	R (kPa)	h_a (Mpa)	c_r (-)	S_u (kPa)	h (m)
6	1016.3	2	0.4	8	2000	1600	725	4.5
5	1205.7	2	0.4	7	2000	2162	538	6
4	1400	2	0.4	8	2300	2150	625	4
3	1877	2.2	0.4	11	3100	2150	838	4
2	3942.4	2.2	0.4	23	6500	2150	1760	12
1	6838.3	2.65	0.4	40	11,000	2150	3053	4

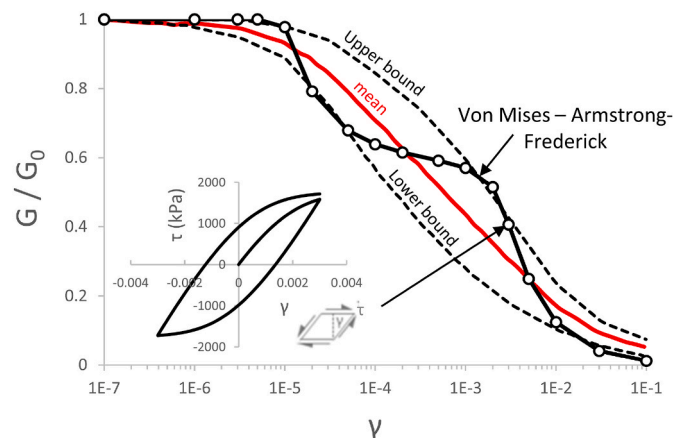


Fig. 5. Nonlinear soil response modelled with a von Mises-Armstrong-Frederick soil model, for $G_0/S_u = 800$. Comparison of computed $G/G_0 - \gamma$ degradation curves with the experimental curves from the specific site for the 2nd soil layer (Table 2). The inset plots the shear stress-strain ($\tau - \gamma$) hysteresis loops for $\gamma = 0.003$. Nearly identical plots are obtained for the remaining soil layers.

degree of inelasticity is expected.

2.5. Interfaces

In the simplest elastic model, all interfaces (reactor building-soil and auxiliary building-soil) are modelled as tied. However, during strong seismic shaking, the soil-structure interfaces may be subjected to foundation uplifting and sliding, which can alter the dynamic response of the structures. As it will be demonstrated later, these nonlinear interface effects may not necessarily result in a reduction of the seismic response compared to the tied (linear) interfaces. Real-ESSI provides different types of interface elements with increasing complexity. A zero-length, stress-based, dry contact element with nonlinear hardening shear behavior called StressBasedSoftContact_NonLinHardShear [49, 50] is adopted for the present study. Such contact model allows simulation of interface behavior in both normal and tangential directions to the contact surface. In the normal (vertical) direction, a nonlinear elastic penalty stiffness function representing a soft contact with stiffness increasing exponentially with penetration is used to model the contact behavior (Fig. 7a). This is considered a realistic representation of the normal soil-structure interface behavior, as the normal contact force changes gradually upon contact and becomes zero upon detachment. For the nonlinear contact behavior in the tangential (horizontal) direction, an Armstrong-Frederick nonlinear hardening model is used, where the shear stress to normal stress ratio ($\mu = \tau/\sigma_n$) increases nonlinearly from 0 to the value of the residual friction coefficient μ_r (Fig. 7b).

Due to the lack of experimental data for the NPP soil-structure interfaces, reasonable engineering assumptions were made to calibrate the parameters of the interface model. The input parameters used in the model are listed in Table 3, where k_{n0} , sr , $k_{n,max}$, and h correspond to the initial normal stiffness, the normal stiffness stiffening rate, the maximum normal stiffness, and the shear zone thickness, respectively. These parameters control the stiffness behavior of the interface in the normal direction and result in negligible penetration, of the order of 1×10^{-3} mm. The response in the tangential direction is controlled by the shear stiffness $k_t^{\sigma_{n0}}$ at $\sigma_{n0} = 101$ kPa normal stress (i.e., shear stiffness k_t depends on the normal stress and is equal to $k_t^{\sigma_{n0}}$ when the normal stress σ_n is equal to $\sigma_{n0} = 101$ kPa), the residual friction coefficient μ_r , which is set to 0.6, and the shear zone thickness h , which is set to 1 mm, as it is

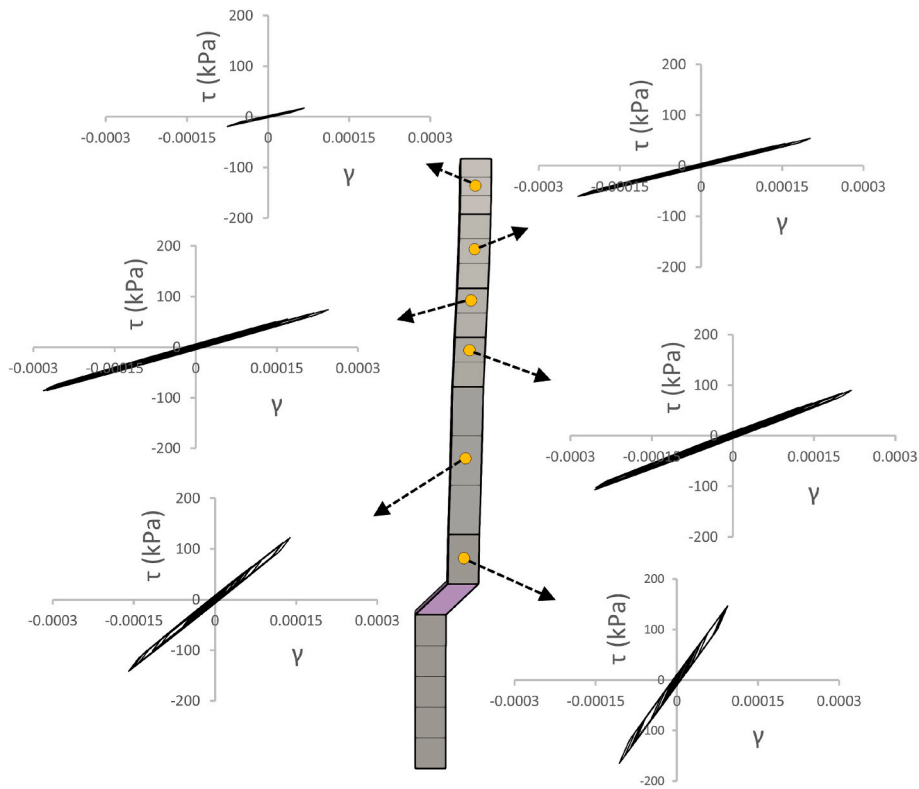


Fig. 6. Dynamic response of nonlinear soil column: shear stress–strain ($\tau - \gamma$) hysteresis loops for each soil layer.

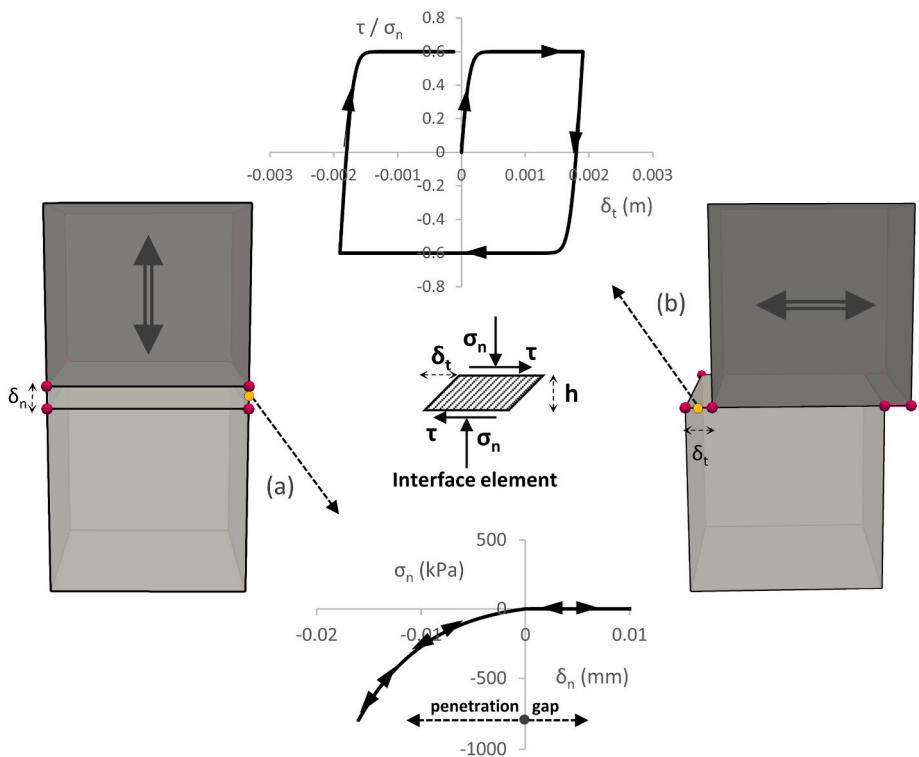


Fig. 7. Cyclic response of the nonlinear interface elements used in this study: (a) normal stress–normal displacement ($\sigma_n - \delta_n$); and (b) shear stress over normal stress ratio–shear displacement ($\tau / \sigma_n - \delta_t$) response.

typically assumed to be 5–10 times the mean soil particle diameter D_{50} [51]. A simple example of shear behavior between two elastic brick elements subjected to static cyclic shear excitation, after application of a

vertical stress of 600 kPa (which is representative of the vertical stress below the foundation of the reactor building) is shown in Fig. 7b. It is essential to use a sufficiently high value of k_t to reach the residual

Table 3
Input parameters of the nonlinear interface model.

k_{n0} (MPa)	sr (-)	$k_{n,max}$ (MPa)	k_t^{no} (kPa)	c_n (kPa*s)	c_t (kPa*s)	h (mm)	μ_r (-)
500	100	2500	1000	0.5	4	1	0.6

friction coefficient after reasonable shear displacement δ_t (here approximately 0.3 mm). However, excessively high values of k_t could lead to numerical convergence problems, so a compromise is required. To support numerical stability and to serve as a physical energy-dissipation mechanism, the interface model provides two additional parameters c_n and c_t , which correspond to the viscous damping in the normal and tangential directions, respectively. These parameters represent the viscous energy dissipation that can occur at the soil–structure interface during the opening and closing of the gap, as the fluids (air or water) interact with the structure. Parametric analyses indicated that a shear viscous damping of 4 kPa*s and a normal viscous damping of 0.5 kPa*s provide numerical convergence without compromising the reliability of the results for the studied problem.

In the absence of experimental data to properly calibrate the interface model, the chosen parameters were derived using a combination of engineering expertise and parametric analyses, assessing the impact of each parameter on the structural response for the studied problem. As such, these parameters should not be blindly applied in future studies. For the design or re-evaluation of a real NPP, the engineer should carefully calibrate the interface model parameters to be representative of the various interfaces of the site-specific project (e.g., concrete to soil, waterproofing to soil, concrete basemat to concrete mudmat, etc.). To obtain a comprehensive understanding of the interface model described in this paper, the readers are encouraged to refer to Sinha [50].

3. Elastic soil and tied interfaces

3.1. The effect of SSI

Even today, SSI effects are often neglected in the design or assessment of conventional structures, as it is assumed that they are beneficial. This assumption is based on the expectation that the soil will absorb a significant portion of the seismic energy, primarily through its material and radiation damping, that would have otherwise been absorbed by the

structure. However, a structure sitting on a flexible soil base will experience a shift of its vibration modes to lower frequencies, and depending on the structure and the seismic excitation, the seismic demand from these new fundamental frequencies could be detrimental. To illustrate this, Fig. 8 compares the response of a fixed-base model of the NPP reactor building, in which the selected horizontal motion is applied at its base, with the full SSI model where the DRM is used to generate the same motion at the ground surface. The top node horizontal acceleration time history responses of the external NPP containment walls are plotted at the top (Fig. 8b), accompanied by their respective elastic horizontal response spectra at 5 % damping (SA) at the bottom (Fig. 8c). The peak of the black curve (no SSI) at around 4 Hz corresponds to the first vibration mode of the external walls obtained by eigenvalue analysis (see Fig. 2). Accounting for elastic SSI leads to a dramatic reduction of this peak. Hence the general belief that neglecting SSI is conservative. At the same time, however, a new vibration mode appears at around 2 Hz (related to the rigid body rocking motion of the reactor building on a flexible base), where the seismic demand is significantly higher than the corresponding demand without SSI (Fig. 8a). Such rocking motion cannot be predicted by assuming a fixed-base model. Obviously, the seismic demand from the ignored rocking of the reactor building could potentially compromise its safety, calling for a proper investigation that accounts for SSI.

3.2. The effect of the auxiliary building on the reactor building (SSSI)

The main goal of this study is to explore the significance of SSSI modelling. SSSI can have either positive or negative effects on the response of the structure, which in turn can affect the seismic demand on the installed components. To this end, the dynamic effect of the auxiliary building on the reactor building is first studied, assuming tied interfaces and elastic soil conditions. Fig. 9 presents the elastic spectral acceleration (SA) in horizontal direction at 5 % damping for seven critical points of the reactor building, with and without the presence of the auxiliary building (i.e., with and without SSSI). Point 1 is at the center of the foundation, points 2 and 3 are on the RV, point 4 is at the top of the WP, point 5 is at the inner side of the internal containment wall at a height where usually a crane is attached, and points 6 and 7 are at the top of the internal and external containment walls, respectively. The SA at the top of the auxiliary building is also plotted (point 8), having a clear peak close to 4 Hz related to its horizontal translational motion. This is

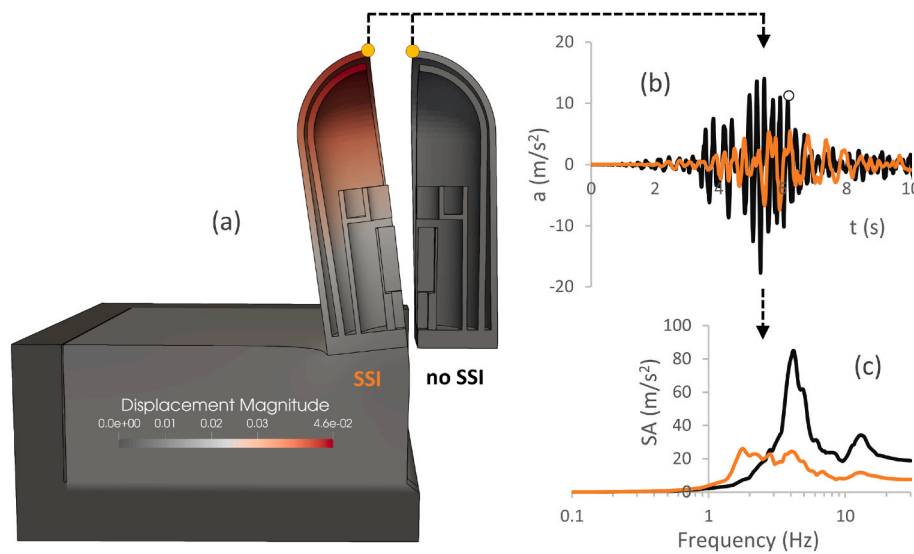


Fig. 8. The effect of elastic SSI on the horizontal response of the external NPP containment wall of the reactor building. Comparison of the fixed-base model to the one that accounts for elastic SSI: (a) snapshot of displacement contours at $t = 6.2$ s (scale factor 300); (b) horizontal acceleration time histories of the top node of the external walls; and (c) the corresponding horizontal elastic acceleration response spectra.

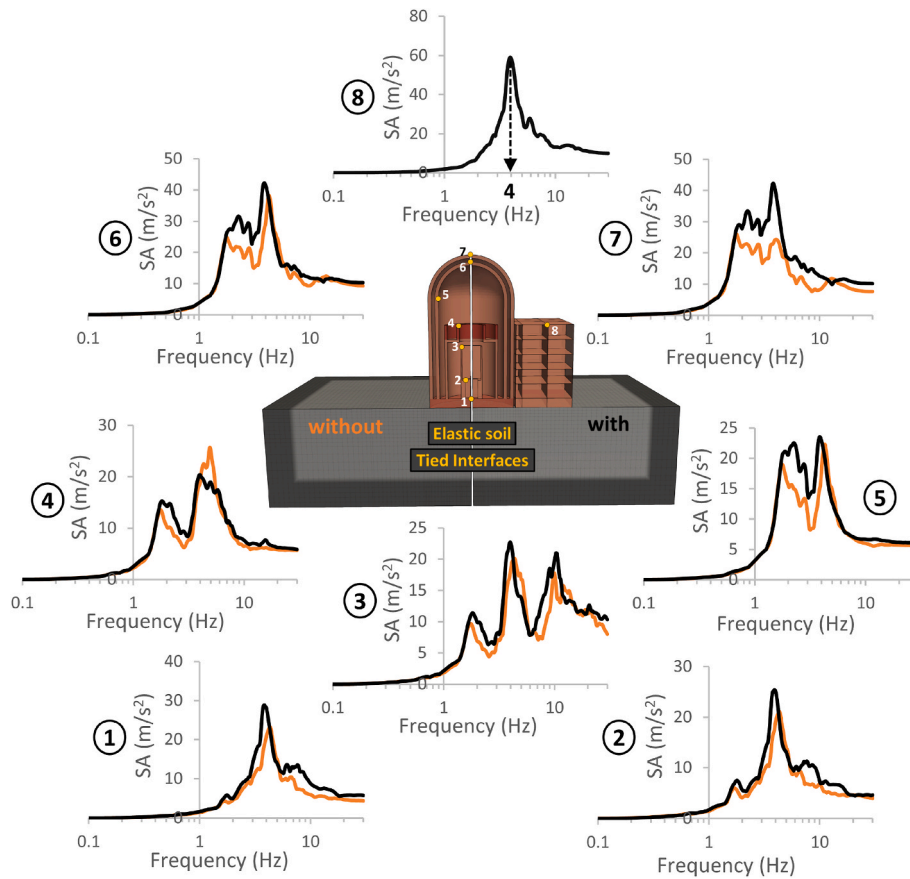


Fig. 9. Elastic soil and tied interfaces. The effect of SSSI on the response of the reactor building. Comparison of the elastic horizontal acceleration response spectra SA at critical points of interest on the reactor building, “with” and “without” the presence of the auxiliary building.

significantly smaller than the 6.2 Hz eigenfrequency of the auxiliary building obtained from the eigenvalue analysis for the fixed-base case (Fig. 3), and is due to the flexible soil base. A noteworthy observation in Fig. 9 is the overall increase in SA values caused by the presence of the auxiliary building for the majority of the investigated points of the reactor building, particularly close to the auxiliary’s building resonant frequency (see e.g. point 7 at 4 Hz).

This amplification in the response of the reactor building is attributed to the out-of-phase rocking motion of the two buildings, as clearly shown in Fig. 10 which plots the soil deviatoric effective stress contours for the two cases. Notice the stress increase beneath the adjacent edges of the foundations of the two structures caused by the additional amount

of vertical pressure due to the out-of-phase rocking motion of the auxiliary building. This visibly increases the rotation of the reactor building, leading to acceleration amplifications, particularly for its rocking-prone parts, such as the external containment wall (point 7). This result is consistent with the earlier work of Roesset et al. [11], where it was shown that the rocking of one structure can be significantly altered in the presence of another nearby structure.

The above comparison in terms of SA values inherently depends on the selected excitation. To solely focus on how the dynamic characteristics of the reactor building are modified due to the presence of the auxiliary building, Fig. 11 plots the horizontal acceleration transfer functions for points 4 and 7 with respect to point 1 comparing the two

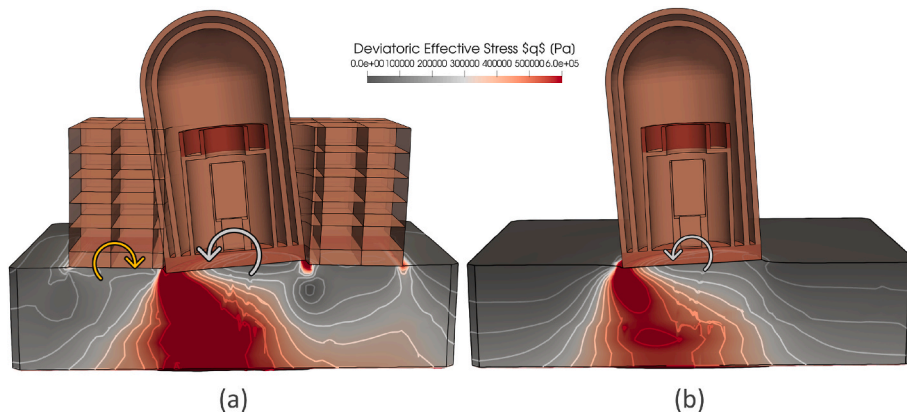


Fig. 10. Elastic soil and tied interfaces. Snapshots of deviatoric effective stress contours: (a) “with”; and (b) “without” the auxiliary building at $t = 5.58$ s (scale factor 200). The out-of-phase rotational coupling between the two buildings leads to an aggravation of the seismic response of the reactor building.

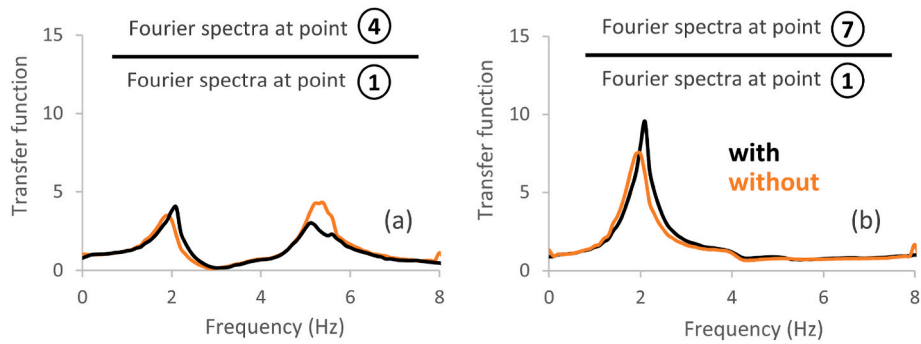


Fig. 11. Elastic soil and tied interfaces. Horizontal acceleration transfer functions with respect to point 1 for: (a) point 4; and (b) point 7; “with” and “without” the auxiliary building. The acceleration response time histories were multiplied with a Hamming window before calculating the corresponding Fourier spectra to reduce spectral leakage.

models. As also shown in Fig. 9, the auxiliary building amplifies the rocking vibration mode of the reactor building at around 2 Hz. The reduction between 5 and 6 Hz for point 4 agrees with Fig. 9 too, and is associated with the beneficial out-of-phase interaction between the two buildings, which is explained in detail later.

3.3. Vibration behavior analogous to seismic resonant metamaterials

At this point, it is worth drawing an analogy between the out-of-phase amplification mechanism of the auxiliary building and the out-of-phase response attenuation mechanism of seismic resonant metamaterials. As shown by Kanellopoulos et al. [52], the seismic response of a horizontally vibrating building can be reduced by introducing multiple horizontal resonators into the ground adjacent to the building. These resonators are tuned to vibrate out-of-phase with the ground at the frequency of interest (i.e., the resonant frequency of the building). In this

case, the out-of-phase horizontal forces from the resonant metamaterials are beneficial to the building, as they oppose the horizontal forces from the seismic waves. Thus, if it were possible here to restrain the rotations and allow only the horizontal translational motion of the auxiliary building and the reactor building, their out-of-phase interaction would actually benefit the reactor building. As it will be shown later, when soil inelasticity is considered, the rocking motion of the soil–buildings system is suppressed once the soil yields, and the horizontal out-of-phase mechanism begins dominating over the rocking one, favoring the beneficial interaction between the two buildings.

4. Elastic soil and nonlinear interfaces

4.1. The effect of nonlinear interfaces

The NPP model sophistication is enhanced by introducing the

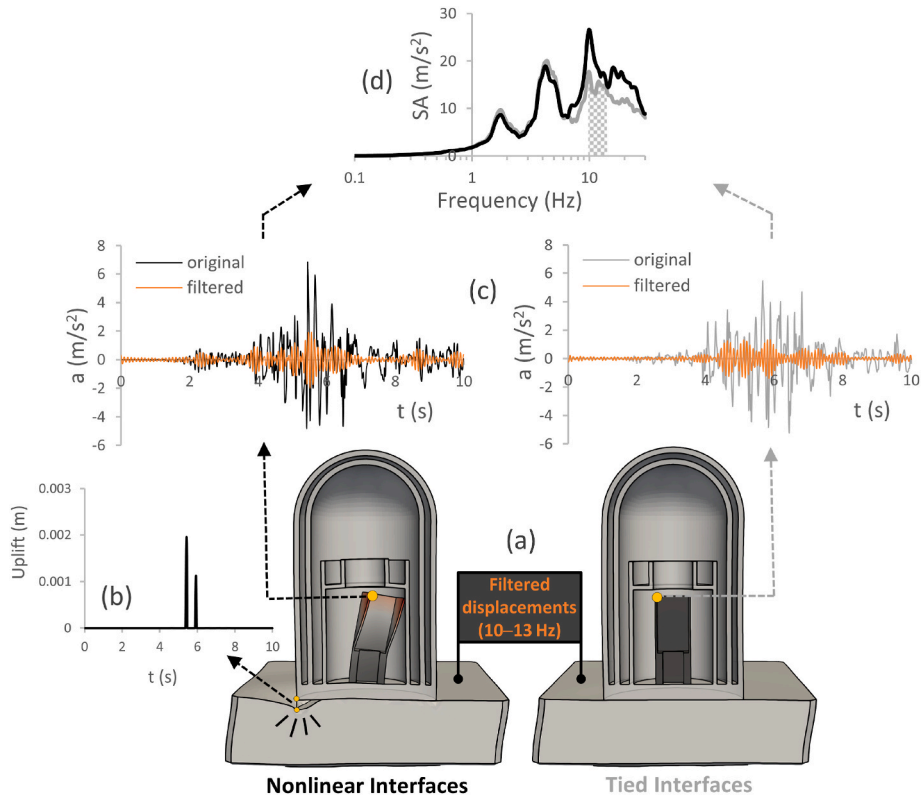


Fig. 12. The effect of nonlinear interfaces on the RV’s response in the absence of the auxiliary building. Comparison with the case of tied interfaces: (a) snapshot of filtered vertical displacement contours (10–13 Hz) at $t = 5.5$ s (scale factor 20,000); (b) time history of uplifting at the left edge of the foundation; (c) filtered and original horizontal acceleration time histories of the RV’s top; and (d) the corresponding elastic horizontal acceleration response spectra.

previously discussed nonlinear interface at the soil–reactor building and soil–auxiliary building contacts. The effect of the nonlinear interface on the dynamic response of the reactor building is evaluated by comparison with the tied interface cases. Initially, the auxiliary building is omitted to focus on the effect of the nonlinear interface on the response of the reactor building. The nonlinear interfaces lead to a small decrease in SA at the 7 characteristic points (not shown here), 10 % or less for frequencies below 10 Hz. This insignificant effect is due to the negligible amount of sliding at the soil–foundation interface (of the order of 1–2 mm), which implies a negligible amount of energy dissipation. Interestingly, the nonlinear interface has a notable effect on the SA of point 3 (top of the RV) at its resonant frequency of 10 Hz (recall from Fig. 2 that its fixed-base resonant frequency is about 12 Hz), causing a significant SA amplification of about 50 %. This is depicted in Fig. 12d, along with cross-sectional views of the compared models (Fig. 12a) displaying the 10–13 Hz filtered displacement field of interest (for this, first the unfiltered displacements of all nodes are extracted, then subjected to a bandpass filter from 10 to 13 Hz, and finally reconstructed into ParaView compatible files to visualize the filtered displacement field). Additionally, notice the uplifting of the foundation from the soil with its corresponding uplifting time history diagram (Fig. 12b). As can be visibly inferred by comparing the deformation of the RV for the two cases, this opening and closing of the gap at the soil–foundation interface introduces higher frequency vibrations to the reactor building foundation, leading to the observed amplification of SA at RV’s top. The horizontal acceleration time history diagrams of the RV’s top points (Fig. 12c) further confirm this observation, showing an increase in the 10–13 Hz filtered acceleration time history plots of the nonlinear interface case after 5.5 s and 6 s, when the gap opens and closes twice.

The next step is to compare the responses of the complete 3D NPP models, including the auxiliary building, with a nonlinear and with a tied interface. By doing so, the effect of the nonlinear interfaces on the reactor–auxiliary building interaction can be estimated. The cross-sectional views of Fig. 13a compare the two cases, displaying a decrease of displacement of both buildings when the nonlinear interface is considered. The rotations of the buildings are also visibly decreased due to some sliding. The zoomed-in plots highlight the sliding of the

auxiliary building. The reduction of the peak in the SA of point 8, due to the energy dissipation at the soil–foundation interface of the auxiliary building, is expected to lead to a reduction of its negative effect on the response of the reactor building (Fig. 13b). Indeed, the comparison of SA at point 7 (top of the external containment wall), indicates that the nonlinear interface leads to a reduction of the detrimental interaction between the two structures. However, it remains to be seen whether the effect of the auxiliary building on the reactor building is completely reversed (from detrimental to beneficial) or is merely reduced (less detrimental).

4.2. The effect of the auxiliary building on the reactor building (SSSI)

The effect of the auxiliary building on the reactor building is assessed by comparing the response of the reactor building in the absence and presence of the auxiliary building, considering nonlinear interfaces for both cases. The SA plots for the points of interest are compared in Fig. 14, as done previously. As expected, the detrimental effect caused by the auxiliary building is suppressed compared to Fig. 9, but is still present for frequencies up to 4 Hz. However, the beneficial horizontal out-of-phase interaction, which is enhanced by interface sliding, starts gaining ground over the rocking interaction, as manifested by the noticeable reduction in SA of the reactor building after 4 Hz (see shaded areas). In addition, the presence of the auxiliary building substantially reduces the high-frequency response of the RV’s top (point 3). This can be explained with the help of Fig. 15, which shows the cross-sectional views of the 10–13 Hz filtered displacement fields of the two models, along with the corresponding filtered horizontal acceleration time histories of point 3 (top of the RV). Notably, the closing of the gap at the left edge of the soil–foundation interface of the standalone reactor building, which was found earlier to amplify the RV’s response at around 10 Hz, is prevented by the opposite motion of the auxiliary building (see zoomed-in plot in Fig. 15a).

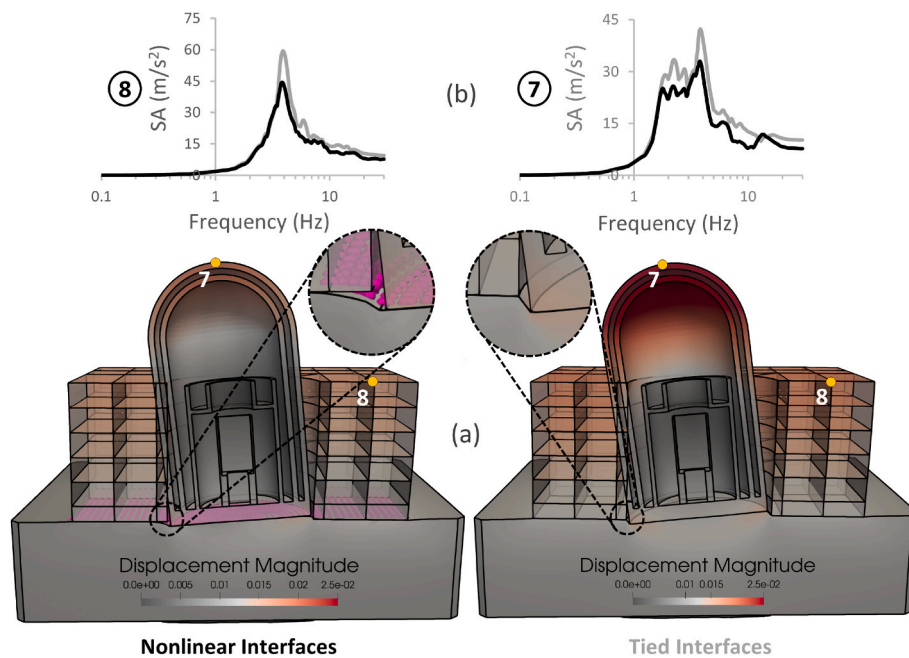


Fig. 13. The effect of nonlinear interfaces on the response of the external wall of the reactor building in the presence of the auxiliary building. Comparison with the case of tied interfaces: (a) snapshot of displacement contours at $t = 5.58$ s (scale factor 200); and (b) elastic horizontal acceleration response spectra at points 7 and 8. The reduction in SA at point 8 caused by the nonlinear interfaces leads to reduction of the negative effect of the auxiliary building on the response of the reactor building.

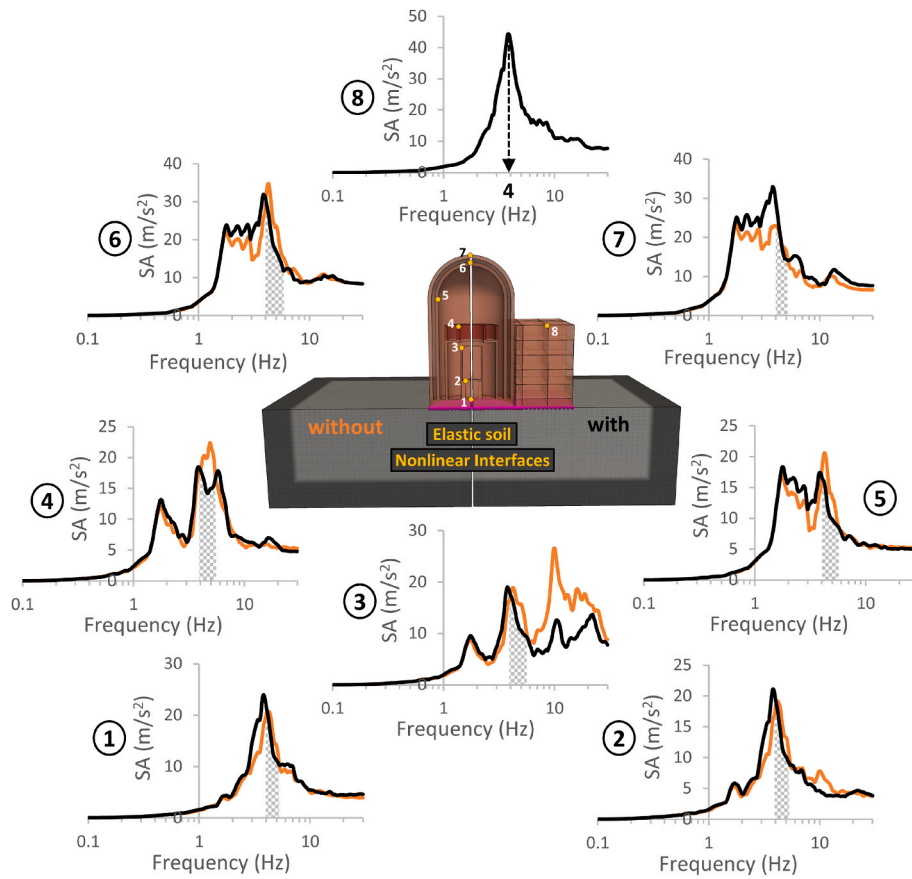


Fig. 14. Elastic soil and nonlinear interfaces. The effect of SSSI on the response of the reactor building. Comparison of the elastic horizontal acceleration response spectra SA at critical points of interest on the reactor building, “with” and “without” the presence of the auxiliary building.

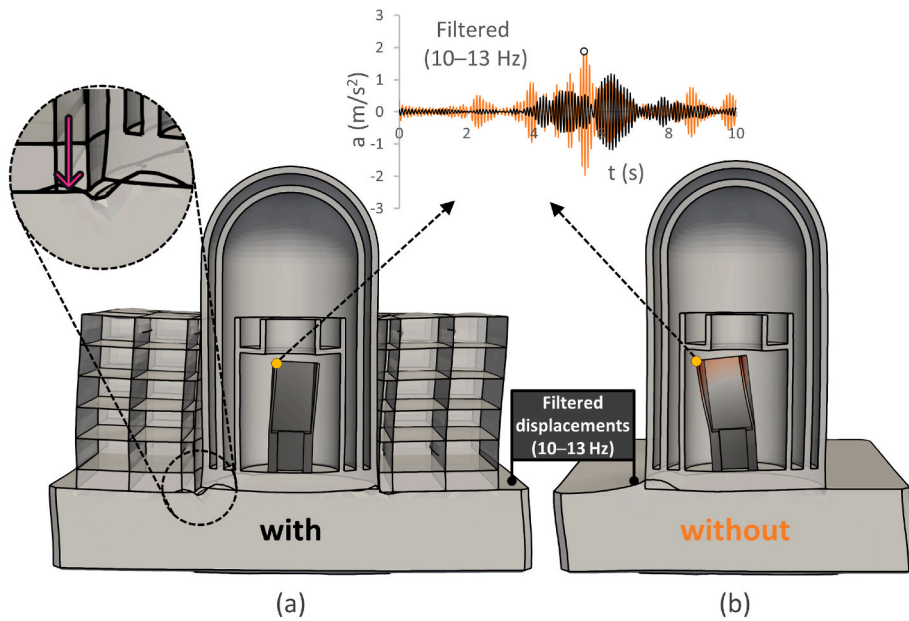


Fig. 15. Elastic soil and nonlinear interfaces. Snapshot of filtered displacement contours (10–13 Hz): (a) “with”; and (b) “without” the presence of the auxiliary building at $t = 5.47$ s (scale factor 20,000). The inset plots the filtered horizontal acceleration time histories at the top of the RV.

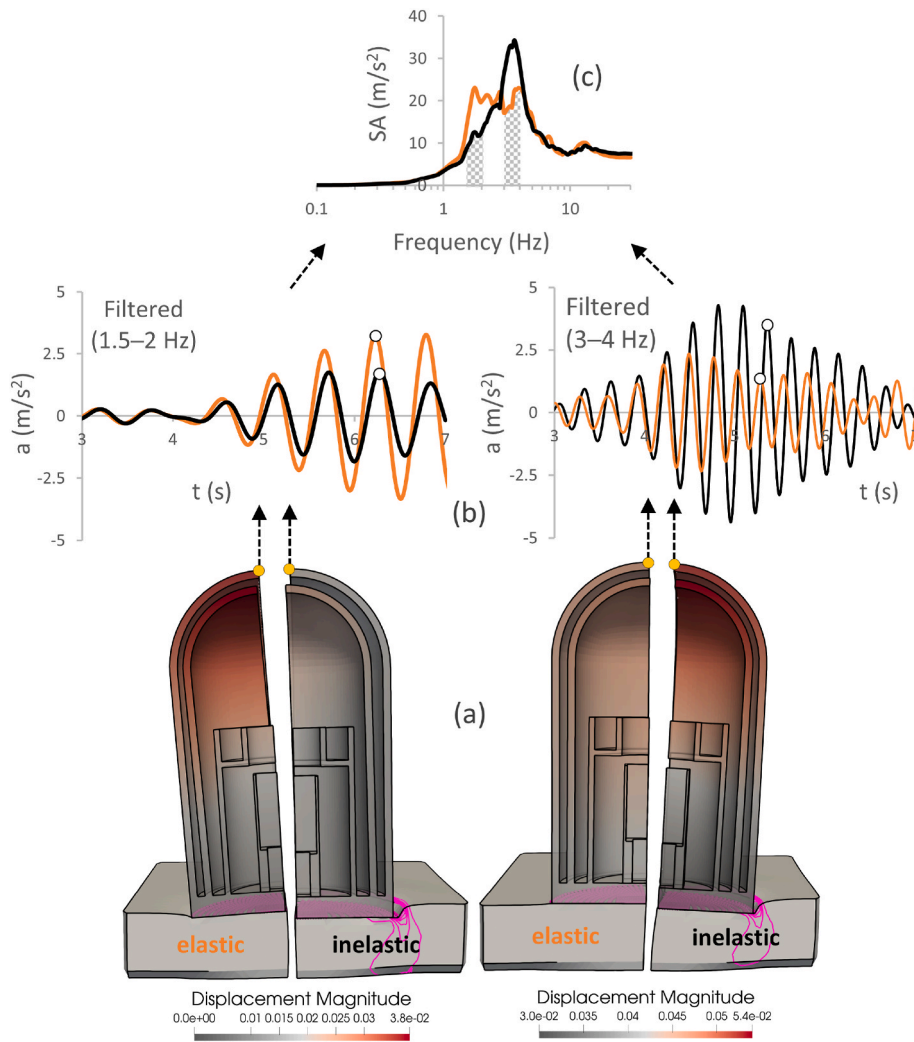


Fig. 16. The effect of soil nonlinearity on the response of the external containment wall in the absence of the auxiliary building. Comparison with the case of elastic soil: (a) snapshots of displacement contours at $t = 6.29$ s (left) and $t = 5.37$ s (right) (scale factor 200); (b) filtered horizontal acceleration time histories at 1.5–2 Hz (left) and 3–4 Hz (right); and (c) the corresponding elastic horizontal acceleration response spectra SA.

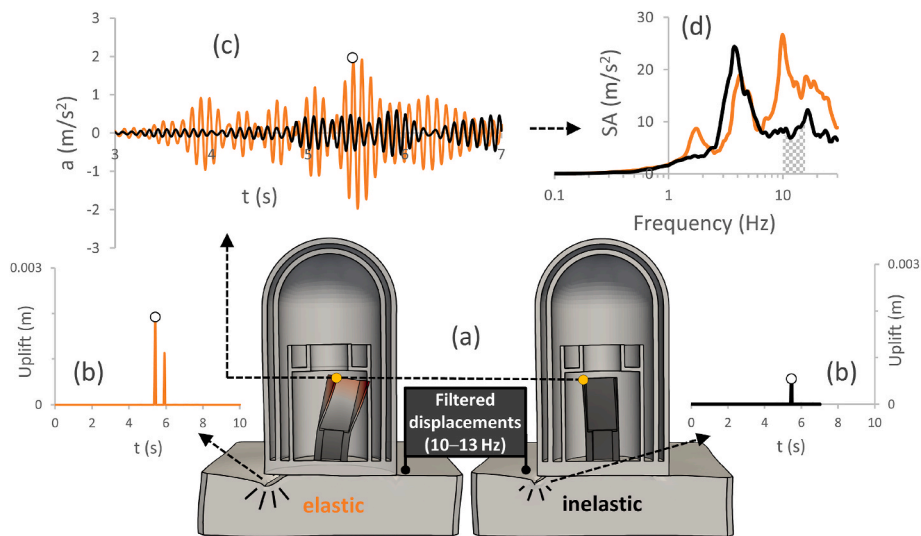


Fig. 17. The effect of soil nonlinearity on the response of the RV in the absence of the auxiliary building. Comparison with the case of elastic soil: (a) snapshot of filtered displacement contours (10–13 Hz) at $t = 5.45$ s (scale factor 20,000); (b) time histories of foundation uplifting; (c) filtered horizontal acceleration time histories at the top of the RV; and (d) the corresponding elastic horizontal acceleration response spectra.

5. Nonlinear soil and nonlinear interfaces

5.1. The effect of soil nonlinearity

The final step in terms of NPP model sophistication enhancement in this study is to account for nonlinear soil response, employing the previously discussed nonlinear constitutive model. The effect of soil nonlinearity is assessed by comparing the dynamic response of the reactor building, with and without soil nonlinearity.

To focus on the role of soil nonlinearity, the auxiliary building is removed. Comparing the SA at the top of the external containment wall for the two cases (Fig. 16c), two interesting observations can be made. First, the rocking, rigid body-like vibration mode of the reactor building with a frequency close to 2 Hz disappears with soil nonlinearity. Second, there is a remarkable increase in the primary bending vibration mode of the reactor building at around 4 Hz. The middle part of the figure (Fig. 16b), which includes the 1.5–2 Hz and 3–4 Hz filtered time history plots, and the corresponding cross-sectional views of the unfiltered displacement magnitude contours at the bottom (Fig. 16a), further assist in understanding these observations. Apparently, the continuing rocking motion of the reactor building is powered (or even amplified) by elastic soil response: every time the foundation rotates, the elastic soil bounces back, pushing the foundation to rotate towards the opposite direction. This is not the case when soil nonlinearity is accounted for, in which case the soil yields and accumulates permanent deformations. Therefore, the rocking motion at 2 Hz is severely suppressed due to soil nonlinearity, leading at the same time to an increase of resonance at a frequency close to 4 Hz.

Regarding the effect of soil nonlinearity on the response of the RV, the previously discussed amplification in the high-frequency range seems to disappear, as shown in Fig. 17d. The cross-sectional views of the 10–13 Hz filtered displacement contours of interest at the bottom (Fig. 17a), in combination with the time histories of foundation uplifting (Fig. 17b), explain the beneficial role of soil nonlinearity. Evidently, soil yielding beneath the foundation leads to accumulation of permanent settlements, resulting in negligible opening and closing of the gap at the interface and dampening of any tendency for high frequency excitation. In the absence of such “gapping” mechanism, the high-frequency

response of the RV cannot be excited.

To assess the influence of soil nonlinearity on the complete NPP model, the auxiliary building is included in the analysis. Fig. 18b compares the SA at the top of the WP (point 4) for the cases of elastic and nonlinear soil (and nonlinear interfaces for both cases), while the SA at the top of the auxiliary building (point 8) are also provided. The reduction of stiffness due to nonlinear soil response leads to a slight shift of the peak SA of point 8 to a lower frequency, while almost maintaining its magnitude. Although the response of the auxiliary building is only slightly affected by soil nonlinearity, the response of the WP is significantly altered, resulting in a significant decrease of SA. As nonlinear soil response suppresses the rocking motion of the system, the previously described horizontal out-of-phase reduction mechanism becomes more prominent, leading to a beneficial interaction between the two buildings, which is responsible for the aforementioned SA reduction. The cross-sectional views of the 3–5 Hz filtered displacement contours at the bottom (Fig. 18a) clearly show the detrimental out-of-phase rotational interaction that prevails in the case of elastic soil, compared to the beneficial out-of-phase horizontal interaction between the two buildings that dominates when soil nonlinearity is accounted for.

5.2. The effect of the auxiliary building on the reactor building (SSSI)

Building on the positive effects of soil nonlinearity, which was shown to improve the dynamic interaction between the two structures, this section aims to evaluate the effect of the auxiliary building on the response of reactor building. In this context, the most sophisticated and realistic models (nonlinear soil and nonlinear interfaces) of this study are used to compare the response of the reactor building, with and without the auxiliary building. A summary of the results is presented in Fig. 19, allowing for several interesting observations. First, the resonant frequency of the auxiliary building (point 8) is reduced from 4 Hz in the elastic soil case to 3.3 Hz, due to soil nonlinearity. Most importantly, the presence of the auxiliary building affects the SA at all points of interest of the reactor building for frequencies higher than the 3.3 Hz resonance (see shaded areas in Fig. 18). Evidently, the nearly shear frame-type behavior of the auxiliary building does not couple well with the external and internal containment walls of the reactor building, which

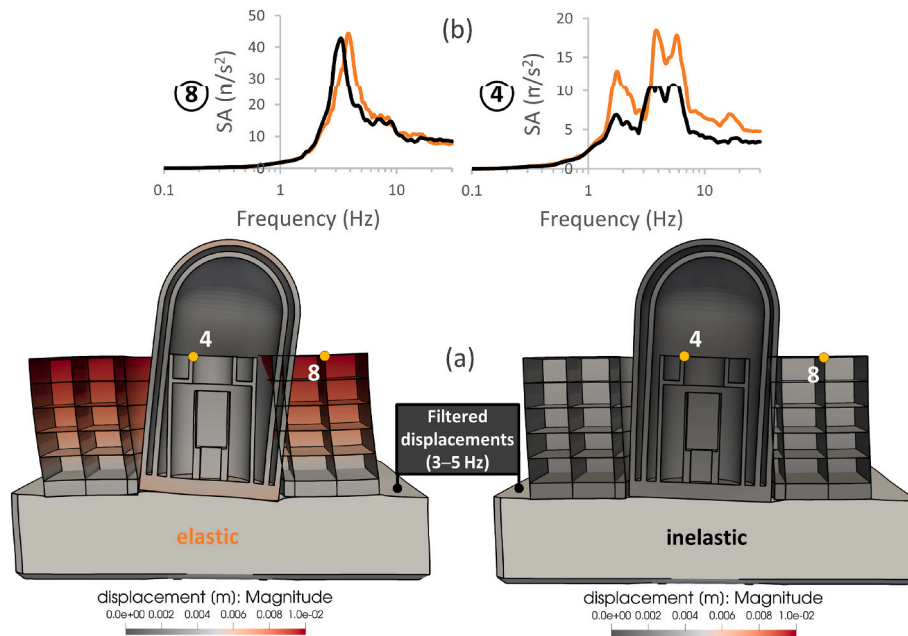


Fig. 18. The effect of soil nonlinearity on the response of the WP in the presence of the auxiliary building. Comparison with the case of elastic soil: (a) snapshot of filtered displacement contours (3–5 Hz) at $t = 5.72$ s (scale factor 700); and (b) elastic horizontal acceleration response spectra (SA) at points 8 and 4. The suppression of the rotational vibration modes caused by soil nonlinearity results in a beneficial out-of-phase horizontal coupling between the two buildings.

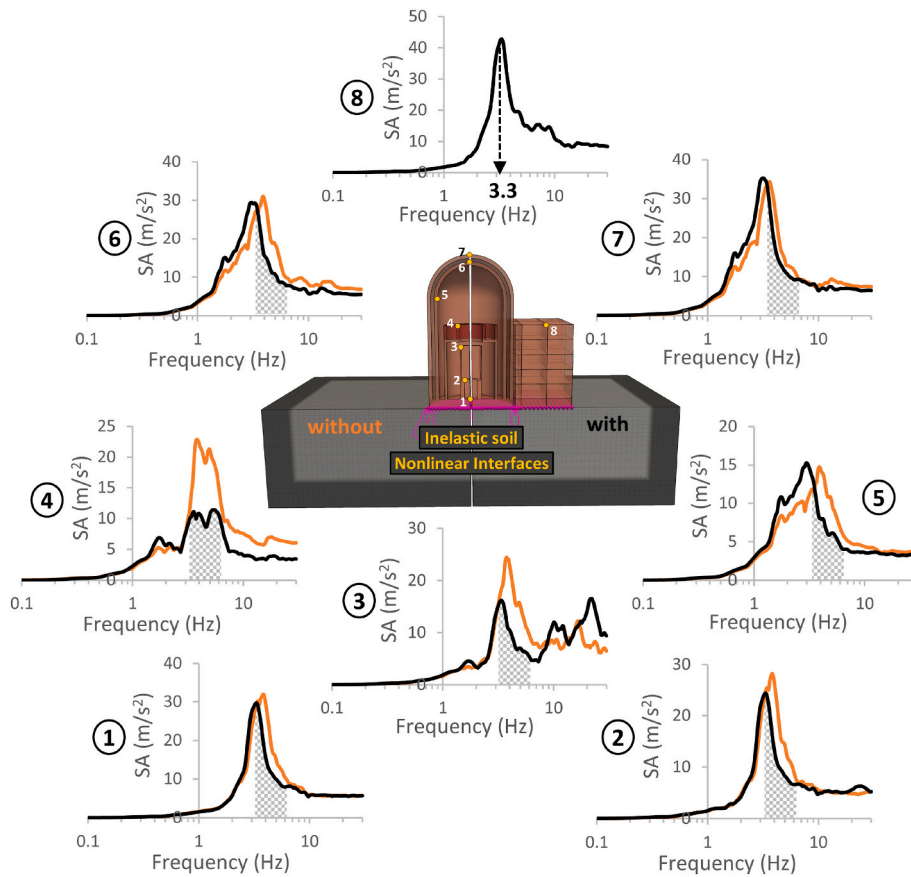


Fig. 19. Nonlinear soil and nonlinear interfaces. The effect of SSSI on the response of the reactor building. Comparison of elastic horizontal acceleration response spectra SA at critical points of interest on the reactor building, “with” and “without” the auxiliary building.

are much taller such that their dynamic response is dominated by their bending vibration modes. Hence, the SA of points 5, 6, and 7 are only slightly shifted to lower frequencies due to the presence of the auxiliary

building, which increases the inertia of the system. This slight decrease of the frequency is in agreement with the experimental results of Kitada et al. [53]. However, a completely different pattern is observed for the

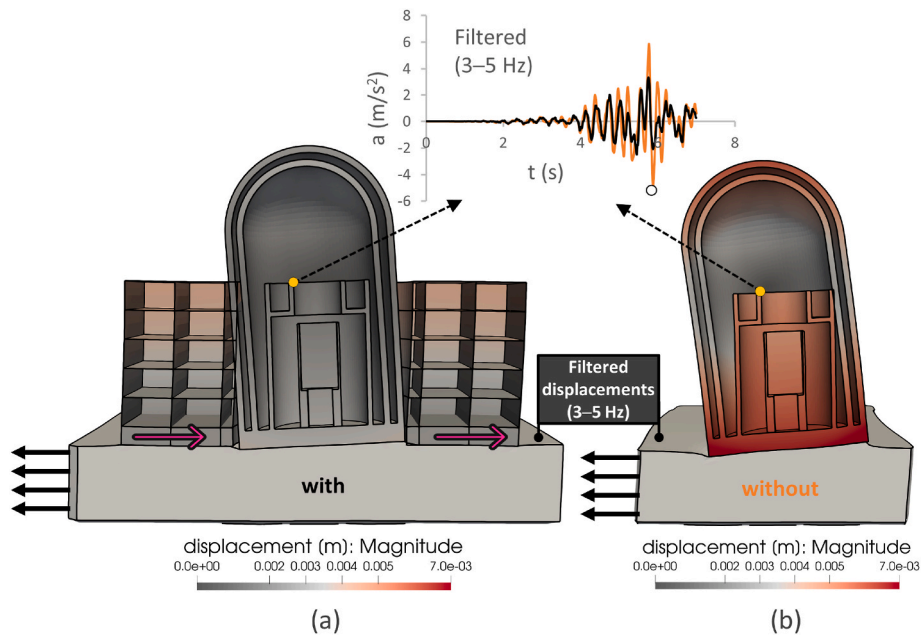


Fig. 20. Nonlinear soil and nonlinear interfaces. Illustration of the beneficial effect of the auxiliary building to the response of the reactor building. Snapshot of filtered displacement contours (3–5 Hz): (a) “with”; and (b) “without” the auxiliary building at $t = 5.87$ s (scale factor 700). The inset plots the horizontal acceleration time histories at the top of the WP. The out-of-phase horizontal coupling between the two buildings is beneficial, reducing the excitation of the reactor building.

remaining points of interest, specifically for the internal CW, the dynamic characteristics (resonant frequency and height) of which are similar to those of the auxiliary building. A remarkable reduction of about 55 % in SA is observed for the top of the WP (point 4). The reduction at the top of the RV (point 3) is of the same order of magnitude, while significant reductions are also observed for the remaining two points of interest.

The last two figures aim to explain the mechanism that enables the auxiliary building to act as a seismic protection “device” for the reactor building, similar to seismic resonant metamaterials. Fig. 20 compares the cross-sectional views of the 3–5 Hz filtered displacement contours, with and without the auxiliary building, along with the corresponding filtered acceleration time histories at the top of the WP (point 4). At the specific snapshot, the soil beneath the two structures starts moving to the left, while at the same time the auxiliary building is moving to the right (a relevant video comparing the two models can be found in the online version of this paper). This out-of-phase oscillation of the auxiliary building relative to the soil, that occurs at frequencies higher than its resonant frequency (3.3 Hz), reduces significantly the horizontal accelerations of the soil at the 3–5 Hz frequency range. This is beneficial for the parts of the reactor building that have resonant vibration modes in this frequency range and, thus, are subjected to reduced dynamic excitation by the soil.

To visualize this out-of-phase mechanism, Fig. 21 compares the displacement vectors in the soil at the same time for the two cases examined, viewed from above. Notice that in the left snapshot (with the auxiliary building) although the soil has started moving to the left, the auxiliary building is still moving to the right pushing the soil to this direction; as a result, the horizontal displacement vectors beneath it point to the right. For the studied low-frequency range, the effect of the structures on the displacement vectors of the soil is localized, disappearing approximately at distance $B/4$ from the auxiliary building (where B is the side length of the auxiliary building; Fig. 21a), and at distance D from the reactor building (where D is the diameter of the reactor building; Fig. 21b). This indicates, as expected, that SSSI effects are not relevant for widely-spaced structures, but do play an important role for closely-spaced structures, such as the ones examined herein. Depending on the importance of the structures, such effects may need to be investigated in more detail. As revealed by the presented results, the effect of SSSI can be beneficial, provided that the structures are properly “tuned”. In the studied idealized problem, this was a mere coincidence, but the implications of the observed *resonant metamaterial-like* response can be far reaching and are worth further consideration.

A final remark on the differential displacements between the two buildings is necessary. Since important equipment (e.g., pipes and other conduits) traverses through the reactor and the auxiliary building, there are strict differential displacement tolerances that must be met. The results presented herein are only meant to provide a crude estimation of the order of magnitude of such differential displacements. For the

specific (idealized) case examined, the vertical differential settlement between the two buildings is of the order of 10 mm, while the maximum horizontal differential displacement (due to sliding at the interfaces) does not exceed 1.5 mm. Finally, the maximum horizontal differential displacement between the two buildings at the top of the auxiliary building is roughly 30 mm for the single horizontal time history used, indicating that if aleatory variabilities (e.g., variability of soil and interface properties, 3D ground motion variability) and epistemic uncertainties are addressed, as in design practice, the structural joint between the two buildings could be closed (pounding). No such pounding was modelled in the analysis, but as previously mentioned, the buildings were spaced at 1 m distance for numerical reasons.

6. Conclusions

A sophisticated 3D FE model of an idealized—but based on existing designs—Nuclear Power Plant (NPP) was simulated in the Real-ESSI Simulator. The NPP consists of the reactor building surrounded by an auxiliary building, each founded on a separate foundation. The primary objective of this proof-of-concept study is to showcase the important role of SSSI modelling (i.e., dynamic interaction between the two buildings) in the assessment of the dynamic response of the reactor building, and in particular, of its critical internal components. The contribution of key aspects of SSSI modelling, such as the soil and interface nonlinearity, is highlighted by gradually increasing the sophistication level of the analysis. Initially, linear elastic soil conditions are assumed and the soil–structure interfaces are tied. Then, special nonlinear interfaces are introduced, allowing for uplifting and sliding at the soil–foundation interfaces. Finally, a simple yet realistic nonlinear constitutive soil model is introduced, suitable for modelling the dynamic cyclic response of pressure-independent materials. The seismic wave field is assumed to consist only of one-component vertically propagating horizontal shear waves (SV), which are inserted into the model using the domain reduction method (DRM), targeting a specific artificial accelerogram at the ground surface. Since only one configuration of structures, spacing between them, soil layers and excitation is considered, the findings of this study are specific to this configuration and, hence, not all of them can be generalized as explained below.

The key findings of the study are summarized as follows:

1) Elastic soil and tied interfaces

- In the absence of the auxiliary building, elastic SSI introduces an additional rocking-type vibration mode of the soil–reactor building system at about 2 Hz, which cannot be predicted by a fixed-base model. This implies that the assumption that ignoring SSI is conservative may not be true, calling for more advanced modelling that can account for such effects, especially in the case of structures of high importance, such as NPPs.

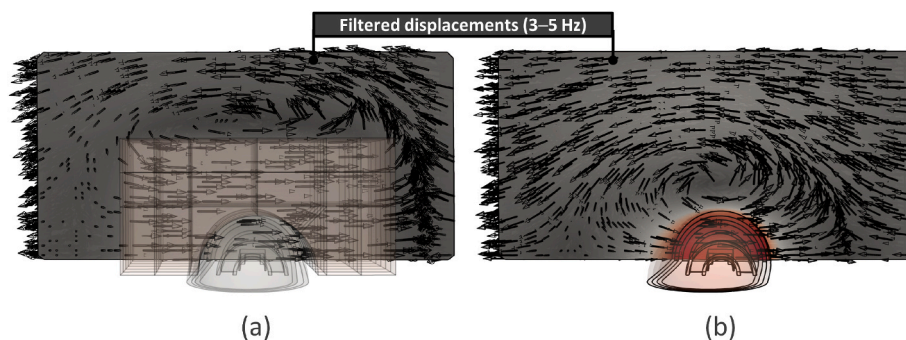


Fig. 21. Nonlinear soil and nonlinear interfaces. Illustration of the beneficial effect of the auxiliary building to the response of the reactor building, both viewed from above. Snapshots of filtered displacement contours (3–5 Hz): (a) “with”; and (b) “without” the auxiliary building at $t = 5.87$ s (scale factor 700). The inset displacement vectors illustrate the beneficial out-of-phase horizontal mechanism provided by the auxiliary building.

- The presence of the auxiliary building and the developing SSSI, leads to an overall amplification of the spectral accelerations SA at characteristic critical points of the reactor building, at frequencies close to the resonance of the auxiliary building. This amplification is associated with a *detrimental out-of-phase rotational interaction* mechanism between the two buildings, which leads to an increase of the rotational response of the reactor building. However, since the out-of-phase rotational interaction between the two buildings depends on the ratio between the wavelength of the incident waves and the distance between the two foundations (as shown in Ref. [18]), this finding is specific for this configuration and cannot be generalized.
- 2) Elastic soil and nonlinear interfaces
- The response is significantly affected by the nonlinear interfaces. During the rocking oscillation of the reactor building, the gapping mechanism (opening and closing) at the soil–foundation interface leads to the development of additional higher-frequency excitations. This unavoidably leads to significant amplifications of response above 10 Hz, which can be *detrimental* for internal components, such as the reactor vessel (RV).
 - The previously mentioned detrimental effect of the auxiliary building on the reactor building due to their out-of-phase rotational interaction is slightly reduced due to limited sliding at the soil–foundation interface of the auxiliary building, which dissipates energy and slightly reduces the response of the auxiliary building.
- 3) Nonlinear soil and nonlinear interfaces
- Nonlinear soil response leads to a significant suppression of the rocking vibration mode of the reactor building. This completely changes the *detrimental out-of-phase rotational interaction* of the two buildings, which now becomes a *beneficial out-of-phase horizontal interaction* for frequencies near and above the resonance of the auxiliary building.
 - Resembling the seismic protection mechanism of *seismic resonant metamaterials*, the auxiliary building essentially protects the reactor building by moving out-of-phase (at its resonant frequency and higher) relative to the soil, thus reducing the excitation of the latter, and consequently the response of critical components inside the reactor building.
 - The components that benefit the most from such *beneficial out-of-phase interaction* between the two buildings are the cylindrical wall (CW) and the RV, which experience a remarkable reduction in spectral accelerations SA of the order of 55 %, in the frequency range associated with the resonant frequency of the auxiliary building.

Summarizing, it should be made clear to the reader that the present study does not aim to provide a generalized analysis method capable of covering all possible aspects in SSSI modelling of NPPs. SSSI is a very complex subject that is sensitive to the site-specific situation. In the opinion of the authors, there can be no generalized method for dealing with all aspects of SSSI. Instead, the study aims to stress the importance of SSSI modelling (including soil and interface nonlinearities) of an idealized NPP, and to point out to aspects of SSSI modelling that can be generalized. As shown, SSSI effects can be either *beneficial* or *detrimental* for the response of the structure, but since they are site- and structure-specific, they cannot be known a priori. In other words, what was found to be detrimental for this configuration can be beneficial for another configuration of structures and vice versa. Thus, engineers should be able to gradually increase the sophistication level of their models, as shown in this study, in order to properly address such complex SSSI effects.

Finally, the observed *beneficial* effects of SSSI between the reactor and the auxiliary building, acting in a similar manner as *resonant metamaterials*, underlines the importance of accounting for such effects in the design of new and the evaluation of existing structures of critical importance, such as NPPs. Optimizing the dynamic characteristics of

neighboring structures, aiming to maximize their beneficial SSSI, may lead to more earthquake-resilient future NPP designs, featuring tuned ensembles of building clusters, optimized to reduce the combined seismic risk.

CRediT authorship contribution statement

Constantinos Kanellopoulos: Writing – review & editing, Writing – original draft, Visualization, Validation, Software, Project administration, Methodology, Formal analysis, Data curation, Conceptualization. **Peter Rangelow:** Writing – review & editing, Supervision, Methodology, Conceptualization. **Boris Jeremic:** Software. **Ioannis Anastasopoulos:** Writing – review & editing, Supervision, Resources, Funding acquisition. **Bozidar Stojadinovic:** Writing – review & editing, Supervision, Resources, Project administration, Funding acquisition.

Declaration of competing interest

The authors declare that they have no known competing financial interests or personal relationships that could have appeared to influence the work reported in this paper.

Data availability

The scripts and files used for this work are deposited in public repositories (see References in Manuscript)

Acknowledgements

This research was part of the project ‘INSPIRE’ funded by the European Union’s Horizon 2020 Research and Innovation Programme under the Marie Skłodowska-Curie grant agreement no. 813424. Additional support from ETH Zurich and University of California Davis is gratefully acknowledged.

Appendix A — Supplementary data

The input files, as well as the pre-and-postprocessing python scripts developed for this paper, have been archived in the ETH Research Collection [54] and ETH Data Archive Deposit (only the scripts) [55,56]. The latest versions of these python scripts are also available on GitHub (<https://github.com/ConstantinosKanellopoulos>). Supplementary data to this article (video) can also be found online at <https://doi.org/10.1016/j.soildyn.2024.108631>.

References

- [1] Mylonakis G, Gazetas G. Seismic soil–structure interaction: beneficial or detrimental? *J Earthq Eng* 2000;4:277–301. <https://doi.org/10.1080/13632460009350372>.
- [2] Anastasopoulos I, Gerolymos N, Drosos V, Kourkoulis R, Georgarakos T, Gazetas G. Nonlinear response of deep immersed tunnel to strong seismic shaking. *J Geotechn Geoenviron Eng* 2007;133:1067–90.
- [3] Anastasopoulos I, Gazetas G, Loli M, Apostolou M, Gerolymos N. Soil failure can be used for seismic protection of structures. *Bull Earthq Eng* 2010;8:309–26. <https://doi.org/10.1007/s10518-009-9145-2>.
- [4] Sakellariadis L, Anastasopoulos I, Gazetas G. Fukae bridge collapse (Kobe 1995) revisited: new insights. *Soils Found* 2020;60:1450–67. <https://doi.org/10.1016/j.sandf.2020.09.005>.
- [5] Sakellariadis L, Anastasopoulos I. On the mechanisms governing the response of pile groups under combined VHM loading. *Geotechnique* 2022;1–22. <https://doi.org/10.1680/jgeot.21.00236>.
- [6] Mantakas A, Tsatsis A, Loli M, Kourkoulis R, Gazetas G. Seismic response of a motorway bridge founded in an active landslide: a case study. *Bull Earthq Eng* 2023;21:605–32. <https://doi.org/10.1007/s10518-022-01544-3>.
- [7] MacCalden PB. Transmission of steady-state vibrations between rigid circular foundations. Los Angeles PP - United States - California: University of California; 1969.
- [8] Warburton GB, Richardson JD, Webster JJ. Forced vibrations of two masses on an elastic half space. *J Appl Mech* 1971;38:148–56. <https://doi.org/10.1115/1.3408735>.

- [9] Luco JE, Contesse L. Dynamic structure-soil-structure interaction. *Bull Seismol Soc Am* 1973;63:1289–303. <https://doi.org/10.1785/BSSA0630041289>.
- [10] Gonzalez JJ, Roesset JM. *Dynamic interaction between adjacent structures*. 1977. Cambridge, Massachusetts 02139.
- [11] Lin H-T, Roesset JM, Tassoulas JL. Dynamic interaction between adjacent foundations. *Earthq Eng Struct Dynam* 1987;15:323–43. <https://doi.org/10.1002/eqe.4290150304>.
- [12] Wang S, Schmid G. Dynamic structure-soil-structure interaction by FEM and BEM. *Comput Mech* 1992;9:347–57. <https://doi.org/10.1007/BF00370014>.
- [13] Qian J, Beskos DE. Harmonic wave response of two 3-D rigid surface foundations. *Soil Dynam Earthq Eng* 1996;15:95–110. [https://doi.org/10.1016/0267-7261\(95\)00026-7](https://doi.org/10.1016/0267-7261(95)00026-7).
- [14] Betti R. Effects of the dynamic cross-interaction in the seismic analysis of multiple embedded foundations. *Earthq Eng Struct Dynam* 1997;26:1005–19. [https://doi.org/10.1002/\(SICI\)1096-9845\(199710\)26:10<1005::AID-EQE690>3.0.CO;2-E](https://doi.org/10.1002/(SICI)1096-9845(199710)26:10<1005::AID-EQE690>3.0.CO;2-E).
- [15] Karabalis DL, Mohammadi M. 3-D dynamic foundation-soil-foundation interaction on layered soil. *Soil Dynam Earthq Eng* 1998;17:139–52. [https://doi.org/10.1016/S0267-7261\(97\)00047-X](https://doi.org/10.1016/S0267-7261(97)00047-X).
- [16] Padrón LA, Aznárez JJ, Maeso O. Dynamic structure–soil–structure interaction between nearby piled buildings under seismic excitation by BEM–FEM model. *Soil Dynam Earthq Eng* 2009;29:1084–96. <https://doi.org/10.1016/j.soildyn.2009.01.001>.
- [17] Liang J, Han B, Todorovska MI, Trifunac MD. 2D dynamic structure-soil-structure interaction for twin buildings in layered half-space I: incident SH-waves. *Soil Dynam Earthq Eng* 2017;102:172–94. <https://doi.org/10.1016/j.soildyn.2017.08.017>.
- [18] Liang J, Han B, Todorovska MI, Trifunac MD. 2D dynamic structure-soil-structure interaction for twin buildings in layered half-space II: incident SV-waves. *Soil Dynam Earthq Eng* 2018;113:356–90. <https://doi.org/10.1016/j.soildyn.2018.05.023>.
- [19] Mason HB, Trombetta NW, Chen Z, Bray JD, Hutchinson TC, Kutter BL. Seismic soil–foundation–structure interaction observed in geotechnical centrifuge experiments. *Soil Dynam Earthq Eng* 2013;48:162–74. <https://doi.org/10.1016/j.soildyn.2013.01.014>.
- [20] Aldaikh H, Alexander NA, Ibraim E, Knappett J. Shake table testing of the dynamic interaction between two and three adjacent buildings (SSSI). *Soil Dynam Earthq Eng* 2016;89:219–32. <https://doi.org/10.1016/j.soildyn.2016.08.012>.
- [21] Bolisetti C, Whittaker AS. Numerical investigations of structure-soil-structure interaction in buildings. *Eng Struct* 2020;215:110709. <https://doi.org/10.1016/j.engstruct.2020.110709>.
- [22] Long H, Wang Z, Zhang C, Zhuang H, Chen W, Peng C. Nonlinear study on the structure-soil-structure interaction of seismic response among high-rise buildings. *Eng Struct* 2021;242:112550. <https://doi.org/10.1016/j.engstruct.2021.112550>.
- [23] Kassas K, Adamidis O, Anastasopoulos I. Structure–soil–structure interaction (SSSI) of adjacent buildings with shallow foundations on liquefiable soil. *Earthq Eng Struct Dynam* 2022;51:2315–34. <https://doi.org/10.1002/eqe.3665>.
- [24] Lee TH, Wesley DA. Soil-structure interaction of nuclear reactor structures considering through-soil coupling between adjacent structures. *Nucl Eng Des* 1973;24:374–87. [https://doi.org/10.1016/0029-5493\(73\)90007-1](https://doi.org/10.1016/0029-5493(73)90007-1).
- [25] Matthees W, Magiera G. A sensitivity study of seismic structure-soil-structure interaction problems for nuclear power plants. *Nucl Eng Des* 1982;73:343–63. [https://doi.org/10.1016/0029-5493\(82\)90011-5](https://doi.org/10.1016/0029-5493(82)90011-5).
- [26] Imamura A, Watanabe T, Yoshida K, Ishizaki M, Motosaka M. *Seismic response characteristics of embedded structures considering cross interaction*. 1991.
- [27] Roy C, Bolourchi S, Eggers D. Significance of structure–soil–structure interaction for closely spaced structures. *Nucl Eng Des* 2015;295:680–7. <https://doi.org/10.1016/j.nucengdes.2015.07.067>.
- [28] Kumar S, Raychowdhury P, Gundlapalli P. Response analysis of a nuclear containment structure with nonlinear soil–structure interaction under bi-directional ground motion. *Int J Adv Struct Eng* 2015;7:211–21. <https://doi.org/10.1007/s40091-015-0092-7>.
- [29] Bolisetti C, Whittaker AS, Coleman JL. Linear and nonlinear soil-structure interaction analysis of buildings and safety-related nuclear structures. *Soil Dynam Earthq Eng* 2018;107:218–33. <https://doi.org/10.1016/j.soildyn.2018.01.026>.
- [30] Van Nguyen D, Kim D, Duy Nguyen D. Nonlinear seismic soil-structure interaction analysis of nuclear reactor building considering the effect of earthquake frequency content. *Structures* 2020;26:901–14. <https://doi.org/10.1016/j.istruc.2020.05.013>.
- [31] Patil G, Choudhury D, Mondal A. Nonlinear dynamic soil–foundation–superstructure interaction analysis for a reactor building supported on a combined piled–raft system. *Int J GeoMech* 2023;23. <https://doi.org/10.1061/JGNAI.GMENG-8096>.
- [32] Jeremić B, Jie G, Cheng Z, Tafazzoli N, Tasiopoulou P, Pisano F, et al. *The real ESSI simulator system*. Davis: Univ California; 2022.
- [33] Geuzaine C, Remacle J-F. *Gmsh: a 3-D finite element mesh generator with built-in pre-and post-processing facilities*. *Int J Numer Methods Eng* 2009;79:1309–31.
- [34] Ahrens J, Geveci B, Law C. *ParaView: an end-user tool for large data visualization*. Elsevier; 2005.
- [35] Bielak J, Loukakis K, Hisada Y, Yoshimura C. Domain reduction method for three-dimensional earthquake modeling in localized regions, part I: theory. *Bull Seismol Soc Am* 2003;93:817–24. <https://doi.org/10.1785/0120010251>.
- [36] Yoshimura C, Bielak J, Hisada Y, Fernández A. Domain reduction method for three-dimensional earthquake modeling in localized regions, part II: verification and applications. *Bull Seismol Soc Am* 2003;93:825–40. <https://doi.org/10.1785/0120010252>.
- [37] *Seismic analysis of safety-related nuclear structures: ASCE/SEI 4-16*. American Society of Civil Engineers; 2017. <https://doi.org/10.1061/9780784413937>.
- [38] Swiss Federal Nuclear Safety Inspectorate E. *Stellungnahme des ENSI zu den aktualisierten Fukushima-Erdbebenachweisen des KKL*. n.d..
- [39] *Seismic design criteria for structures, systems, and components in nuclear facilities: ASCE/SEI 43-19*. American Society of Civil Engineers; 2021. <https://doi.org/10.1061/9780784415405>.
- [40] Zimos D, Vögeli CDM, Szczesiak T, Rangelow P, Mondet Y. *SSI-analysis of nuclear structures in the time-domain using real-ESSI*. 2022.
- [41] Watanabe K, Pisanò F, Jeremić B. Discretization effects in the finite element simulation of seismic waves in elastic and elastic-plastic media. *Eng Comput* 2017;33:519–45. <https://doi.org/10.1007/s00366-016-0488-4>.
- [42] Vucetic M, Dobry R. Effect of soil plasticity on cyclic response. *J Geotech Eng* 1991;117:89–107.
- [43] Puzrin A. *Constitutive modelling in geomechanics: introduction*. Springer Science & Business Media; 2012.
- [44] Moustafa A. Damage-based design earthquake loads for single-degree-of-freedom inelastic structures. *J Struct Eng* 2011;137:456–67. [https://doi.org/10.1061/\(asce\)st.1943-541x.0000074](https://doi.org/10.1061/(asce)st.1943-541x.0000074).
- [45] Frederick CO, Armstrong PJ. A mathematical representation of the multiaxial Bauschinger effect. *Mater A T High Temp* 2007;24:1–26. <https://doi.org/10.1179/096034007X207589>.
- [46] Gazetas G, Anastasopoulos I, Adamidis O, Kontoroupi T. Nonlinear rocking stiffness of foundations. *Soil Dynam Earthq Eng* 2013;47:83–91. <https://doi.org/10.1016/j.soildyn.2012.12.011>.
- [47] Kanellopoulos K, Gazetas G. Vertical static and dynamic pile-to-pile interaction in non-linear soil. *Geotechnique* 2020;70:432–47. <https://doi.org/10.1680/jgeot.18.P.303>.
- [48] Anastasopoulos I, Gelagoti F, Kourkoulis R, Gazetas G. Simplified constitutive model for simulation of cyclic response of shallow foundations: validation against Laboratory tests. *J Geotech Geoenviron Eng* 2011;137:1154–68. [https://doi.org/10.1061/\(ASCE\)GT.1943-5606.0000534](https://doi.org/10.1061/(ASCE)GT.1943-5606.0000534).
- [49] Jeremić B, Yang Z, Cheng Z, Jie G, Tafazzoli N, Preisig M, et al. *Nonlinear finite elements: modeling and simulation of earthquakes, soils, structures and their interaction*. Davis, CA, USA, Lawrence Berkeley Natl. Lab: Univ. California; 2022. Berkeley, CA, USA, 1989-2022. ISBN 978-0-692-19875-9.
- [50] Sinha SK. *Modeling of dry and saturated soil-foundation interfaces*. Davis PP - United States – California: University of California; 2017.
- [51] DeJong JT, White DJ, Randolph MF. Microscale observation and modeling of soil-structure interface behavior using particle image velocimetry. *Soils Found* 2006;46:15–28. <https://doi.org/10.3208/sandf.46.15>.
- [52] Kanellopoulos C, Psycharis N, Yang H, Jeremić B, Anastasopoulos I, Stojadinović B. Seismic resonant metamaterials for the protection of an elastic-plastic SDOF system against vertically propagating seismic shear waves (SH) in nonlinear soil. *Soil Dynam Earthq Eng* 2022;162:107366. <https://doi.org/10.1016/j.soildyn.2022.107366>.
- [53] Kitada Y, Hirotsani T, Iguchi M. Models test on dynamic structure–structure interaction of nuclear power plant buildings. *Nucl Eng Des* 1999;192:205–16. [https://doi.org/10.1016/S0029-5493\(99\)00109-0](https://doi.org/10.1016/S0029-5493(99)00109-0).
- [54] Kanellopoulos C. Dataset for the article: "dynamic structure-soil-structure interaction for nuclear power. *Plants* 2023. <https://doi.org/10.3929/ethz-b-000633093>.
- [55] Kanellopoulos C, Psycharis N, Aguzzi G. *Real-ESSI_postprocessing_tools*. <http://doi.org/10.5905/ethz-1007-704;2023>.
- [56] Kanellopoulos C. *NPP_mesh_generator*. <http://doi.org/10.5905/ethz-1007-703;2023>.